

# Cavity quantum optomechanical nonlinearities and position measurement beyond the breakdown of the linearized approximation

J. Clarke,<sup>1,\*</sup> P. Neveu,<sup>2</sup> K. E. Khosla,<sup>1</sup> E. Verhagen,<sup>2</sup> and M. R. Vanner<sup>1,†</sup>

<sup>1</sup>*QOLS, Blackett Laboratory, Imperial College London, London SW7 2BW, United Kingdom*

<sup>2</sup>*Center for Nanophotonics, AMOLF, Science Park 104, 1098 XG Amsterdam, The Netherlands*

(Dated: August 4, 2023)

Several optomechanics experiments are now entering the highly sought nonlinear regime where optomechanical interactions are large even for low light levels. Within this regime, new quantum phenomena and improved performance may be achieved, however, a corresponding theoretical formalism of cavity quantum optomechanics that captures the nonlinearities of both the radiation-pressure interaction and the cavity response is needed to unlock these capabilities. Here, we develop such a nonlinear cavity quantum optomechanical framework, which we then utilize to propose how position measurement can be performed beyond the breakdown of the linearized approximation. Our proposal utilizes optical general-dyne detection, ranging from single to dual homodyne, to obtain mechanical position information imprinted onto both the optical amplitude and phase quadratures and enables both pulsed and continuous modes of operation. These cavity optomechanical nonlinearities are now being confronted in a growing number of experiments, and our framework will allow a range of advances to be made in e.g. quantum metrology, explorations of the standard quantum limit, and quantum measurement and control.

*Introduction.*—Cavity quantum optomechanics utilizes the cavity-enhanced radiation-pressure interaction to enable precision control of mechanical degrees of freedom. Significant progress has been made in the linearized regime where, for large coherent drives, mechanical displacements give rise to small optical phase shifts. However, there is significant current experimental drive to increase single-photon coupling rates, which necessarily gives rise to the nonlinear response of the cavity and the breakdown of the linearized approximation. Importantly, such behaviour occurs well before the strong single-photon-coupling regime where qualitatively different phenomena may be explored [1–3]. Crucially, due to the nonlinearities of radiation pressure and the cavity response, mechanical displacements give rise to significant rotations to the optical field in phase space and thus the mechanical signal is transduced onto both the phase and amplitude quadratures. This radiation-pressure nonlinearity allows for selective position-squared measurements [4], the generation of macroscopic superposition states [5–7], non-Gaussian entanglement [8–11], and even optomechanical photon blockade for strong single-photon coupling [12, 13]. Recent experimental progress has seen rapid improvements in coupling rates, with cold-atom implementations reaching the strong single-photon coupling regime [14, 15] and, notably even well within the weak single-photon coupling regime, optical rotations have now been observed, which cannot be described by the linearized approximation [16–18].

Closely connected to the radiation-pressure interaction, optomechanical position measurement is a critical component for many research areas ranging from mechanical quantum state engineering to tests of fundamental physics. Prominent example position-measurement applications include ultrasensitive accelerometry [19, 20], yoctogram-resolution mass sensing [21], zeptonewton weak-force sensing [22], single-spin detection [23], and even biomedical

sensing [24]. The precision enabled by cavity optomechanical position measurement also provides a valuable tool for fundamental physics experiments such as gravitational wave detection [25], and searches for new physics [26] including dark matter [27] and non-Newtonian gravity [28].

Owing to the interplay between radiation-pressure back-action and optical quantum noise, optomechanical position measurement is a rich field of study. Prominently, this interplay leads to the standard quantum limit (SQL) [29], which describes restrictions on position measurement sensitivity and is now well understood experimentally [30–32]. Furthermore, within the SQL, weak continuous position measurement [33] combined with feedback [34, 35] can be utilized to cool mechanical oscillators towards their ground state [36, 37]. To go beyond the SQL, back-action evading (BAE) measurements, such as two-tone drive [38–41] or pulses much shorter than the mechanical period [42–45], may be employed. Thus far, the aforementioned position measurement techniques operate in the linearized regime but advances in coupling rates are now forcing experiments to confront the cavity optomechanical nonlinearities.

In this Letter, we develop a framework of optomechanics that accounts for the nonlinearities of both the radiation-pressure interaction and the cavity response. Secondly, we utilize this framework to propose how both pulsed and continuous position measurement can be performed in the nonlinear regime. To measure the mechanical signal transduced onto the optical field we employ the established technique of general-dyne detection [46–48], which ranges from single to dual homodyne. Our formalism allows the optomechanical interaction to be described throughout the entire cavity phase response and enables new regimes of operation, such as the stochastic Gaussian regime we identify and term here. Our framework will enable a broad range of further studies and applications including the important tools of position measurement, squeezing by measurement,

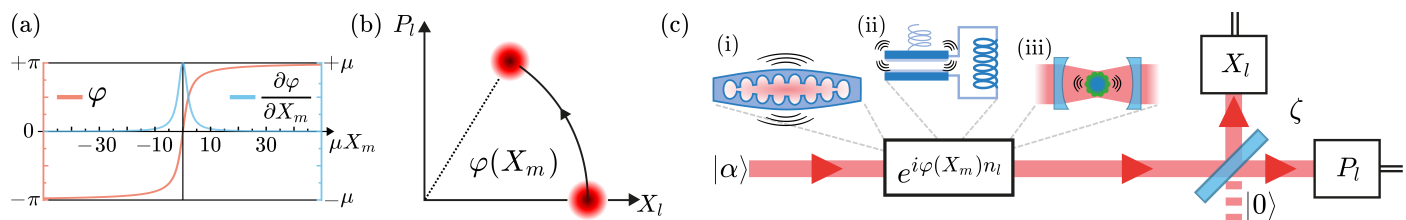


FIG. 1. Cavity quantum optomechanical nonlinearities. (a) Plot of the optical phase  $\varphi(X_m)$  and the dimensionless mechanical momentum kick per photon  $\partial\varphi(X_m)/\partial X_m$  arising from the cavity-enhanced nonlinear optomechanical interaction. Here,  $\mu \propto g_0/\kappa$  is the dimensionless coupling strength,  $X_m$  is the mechanical position quadrature, and the detuning is  $\Delta = 0$ . (b) In optical phase space there is a position-dependent rotation of an input coherent state owing to the nonlinearities of the radiation-pressure interaction and the cavity response. Our framework goes well beyond both the linearized regime, which approximates the rotation as a displacement, and treatments where the interaction is modelled as the unitary  $e^{i\mu n_l X_m}$ , which neglects the cavity response. (c) Position measurement scheme. An optical coherent state  $|\alpha\rangle$  interacts with an optomechanical cavity and is then measured by general-dyne detection, which may be realized with a beamsplitter of variable transmission coefficient  $\zeta$ , vacuum on one input, and amplitude and phase homodyne measurements at the outputs. Our scheme and theoretical formalism are broadly applicable with example nonlinear optomechanical systems including (i) photonic crystals, (ii) microwave LC resonators, and (iii) levitation-based or cold-atom implementations.

and mechanical state tomography to be performed beyond the linearized approximation.

*Nonlinear position measurement scheme.*—Radiation pressure is described by the cubic Hamiltonian  $H/\hbar = -g_0 a^\dagger a (b + b^\dagger)$ , where  $g_0$  is the optomechanical coupling rate, and  $a$  ( $b$ ) is the annihilation operator of the cavity field (mechanical mode). In addition to this nonlinearity, the full response of the cavity itself is also nonlinear, i.e. the optical phase shift depends nonlinearly on the mechanical position and asymptotes to  $\pm\pi$  for large displacements. The combination of these nonlinearities are captured by the Heisenberg-Langevin and input-output equations, which yields the relation  $a_{out} = f(X_m)a_{in}$ , where  $a_{in}$  and  $a_{out}$  are the optical input and output fields and  $f(X_m) = [1 + i(\frac{\mu}{2}X_m + \frac{\Delta}{\kappa})] / [1 - i(\frac{\mu}{2}X_m + \frac{\Delta}{\kappa})]$  is the nonlinear response function. Here,  $X_m$  ( $P_m$ ) is the dimensionless mechanical position (momentum) quadrature,  $\mu = \sqrt{8}g_0/\kappa$  is the nonlinear coupling strength,  $\kappa$  is the cavity amplitude decay rate, which is dominated by external coupling and  $\Delta$  is the detuning from the cavity's resonance at zero mechanical displacement. In Fig. 1(a), we plot the optical phase  $\varphi(X_m) = \arg(f)$  and the dimensionless mechanical momentum kick per photon  $\partial\varphi(X_m)/\partial X_m$  to help visualize these nonlinearities. We then obtain the nonlinear optomechanical unitary  $U = e^{i\varphi(X_m)n_l}$ , where  $n_l$  is the photon number operator of the field entering or leaving the cavity. Notably, for this model, the only approximation made here is that the cavity is adiabatic, i.e.  $\dot{a} \simeq 0$  [49]. Thus, our framework is applicable beyond the linearized regime, and furthermore, overcomes the limitations of previous works that model the optomechanical interaction as  $e^{i\mu n_l X_m}$ , e.g. Refs [50, 51], by accounting for the nonlinear response of the cavity. Fig. 1(b) shows the rotation of an optical coherent state  $|\alpha\rangle$  by angle  $\varphi(X_m)$  following the nonlinear optomechanical interaction, where information about the mechanical position is encoded on both the optical phase  $P_l$  and amplitude  $X_l$  quadratures. The

optical field is then measured by general-dyne detection (cf. Fig. 1(c)), which uses two homodyne detectors to measure both optical quadratures in a proportion controlled by a variable beamsplitter  $B$  with transmission coefficient  $\zeta$ .

*Nonlinear pulsed position measurement.*—A pulsed interaction much shorter than a mechanical period enables a BAE position measurement [42, 43] as the mechanical free evolution (and, indeed, mechanical dissipation) is negligible during this timescale. Such operations require the unresolved sideband regime ( $\kappa \gg \omega_m$ ) to accommodate the pulse within the cavity bandwidth. Here, we consider such a pulsed interaction taking into account the cavity optomechanical nonlinearities. Following the nonlinear interaction  $U$ , the general-dyne measurement outcomes are then used to estimate the mechanical position. The interaction and measurement are described by the measurement operator  $\Upsilon = \langle X_l | \langle P_l | BU |\alpha\rangle |0\rangle$ , which localizes the mechanical state according to  $\rho \rightarrow \Upsilon \rho \Upsilon^\dagger / \mathcal{P}$ , where  $\mathcal{P} = \text{tr}(\Upsilon^\dagger \Upsilon \rho)$  is the probability for the general-dyne outcome  $(X_l, P_l)$ . More explicitly,  $\Upsilon$  is

$$\Upsilon = \frac{1}{\sqrt{\pi}} \exp \left[ -\frac{1}{2} \left( X_l - \sqrt{1 - \zeta^2} X_\alpha f_R \right)^2 - \frac{1}{2} (P_l - \zeta X_\alpha f_I)^2 - i\zeta X_\alpha P_l f_R + i\sqrt{1 - \zeta^2} X_\alpha X_l f_I - \frac{i}{2} (1 - 2\zeta^2) X_\alpha^2 f_R f_I \right], \quad (1)$$

where  $\alpha = X_\alpha/\sqrt{2}$  is the coherent optical amplitude, assumed to be real without loss of generality, and  $f_R = \text{Re}(f(X_m))$  and  $f_I = \text{Im}(f(X_m))$  [49].

We consider a resonant pulsed drive ( $\Delta = 0$ ) and an initial thermal mechanical state with position variance  $\sigma^2 = \langle X_m^2 \rangle = \bar{n} + 1/2$  for mean occupation  $\bar{n}$ . The pulsed interaction gives rise to optical phase-shifts depending on the mechanical position distribution and the nonlinearity of  $\varphi(X_m)$ . Such optical states, with spread determined by  $\mu\sigma$ , are plotted in Fig. 2(a) using the Husimi- $Q$  function. Note that, with increasing  $\mu\sigma$ , the maxima of  $Q$  move away from  $X_l = X_\alpha$  towards  $X_l = -X_\alpha$  and the probability of

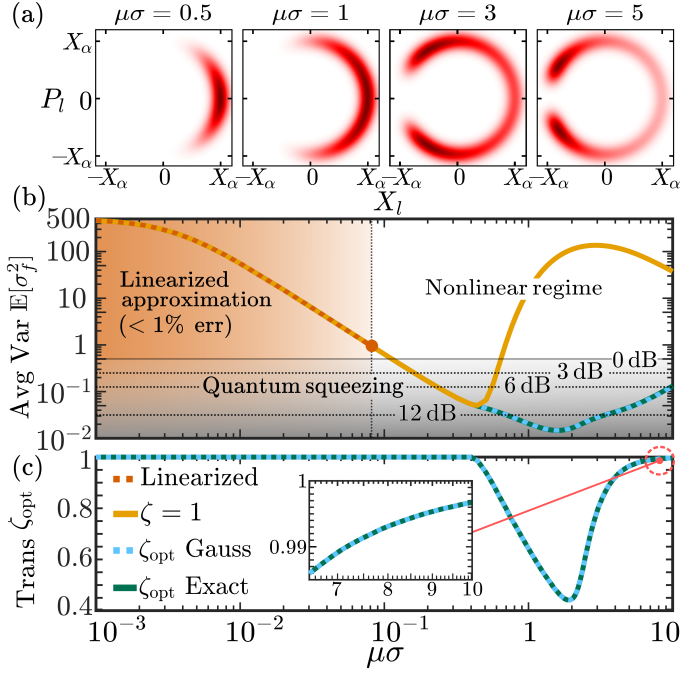


FIG. 2. Nonlinear pulsed position measurement. (a)  $Q$  functions of the optical pulse after the optomechanical interaction for  $X_\alpha = 10$  and increasing  $\mu\sigma$ . For an animation, see the Supplemental Material [49]. (Color scale: white to dark red corresponds to  $Q = 0$  to  $Q = \max(Q)$ .) (b) Plot of the mechanical position variance averaged over all measurement outcomes, using either the optimal general-dyne or a phase-homodyne measurement ( $\zeta = 1$ ), as a function of  $\mu\sigma$  for  $X_\alpha = 200$ , and  $\sigma^2 = 500$ . The grey shaded area indicates quantum squeezing and for these parameters squeezing below 12 dB is achievable using the optimal general-dyne. The orange shaded area indicates where the error from the linearized approximation is less than 1%, which ends at  $\mu\sigma = 0.08$ . (c) Plot of the optimal beamsplitter transmission coefficient  $\zeta_{\text{opt}}$ . Agreement is seen between the exact case and the Gaussian approximation.

landing within the linear response quickly vanishes. In the limit  $\mu\sigma \rightarrow \infty$ , the input coherent state rotates through an angle  $\pm\pi$  in phase space and the mechanical state is unchanged.

Optical loss, including detection inefficiencies, are modelled by a beamsplitter of transmission  $\eta$  placed before the general-dyne detector [52]. As the pulsed unitary  $U$  is a function of mechanical position  $X_m$  alone, optical loss will induce changes in the mechanical momentum [49], while the only effect to the final position marginal is to reduce the strength of the measurement via  $X_\alpha \rightarrow \eta X_\alpha$  in Eq. (1).

The Bayesian inference associated with the general-dyne measurement reduces the mechanical variance from  $\sigma^2$  to  $\sigma_f^2$ , which, in contrast to the linearized regime, depends on the measurement outcome  $(X_l, P_l)$ . As  $X_l$  and  $P_l$  are continuous variables, we average over all measurement outcomes to quantify the performance of reducing the position variance  $E[\sigma_f^2] = \int dX_l \int dP_l \mathcal{P}(X_l, P_l) \sigma_f^2$  [53]. Fig. 2(b) shows the averaged variance  $E[\sigma_f^2]$  as a function

of  $\mu\sigma$  for the optimal beamsplitter transmission coefficient  $\zeta_{\text{opt}}$  demonstrating squeezing well below the ground state width. Here,  $\zeta_{\text{opt}}$  is computed numerically and is plotted in Fig. 2(c) up to a maximum value of  $\mu\sigma$  corresponding to  $g_0/\kappa \approx 0.16$  for the fixed  $\sigma^2 = 500$ . At small and large  $\mu\sigma$ , the  $Q$  function is aligned mostly along the  $P_l$  axis, and hence, the optimal beamsplitter transmission coefficient is close to  $\zeta = 1$ , which agrees with the predictions of the linearized approximation for small  $\mu\sigma$ . While for intermediate  $\mu\sigma$ ,  $Q$  is aligned mostly parallel to the  $X_l$  axis, so the optimal setting is closer to  $\zeta = 0$ . For comparison, Fig. 2(b) also plots  $E[\sigma_f^2]$  for a phase-homodyne measurement  $\zeta = 1$ , which misses the mechanical information encoded on the optical amplitude quadrature causing the averaged variance to grow after  $\mu\sigma \simeq 0.5$ . Thus, despite  $\zeta_{\text{opt}}$  being close to 1 at high  $\mu\sigma$ , the  $E[\sigma_f^2]$  curves for  $\zeta_{\text{opt}}$  and  $\zeta = 1$  still differ and we explore their convergence for even higher values of  $\mu\sigma$  in the Supplemental Material [49]. The nonlinear pulsed model we introduce here enables BAE position measurement well beyond the validity of the linearized regime, even when only the phase quadrature is measured. Moreover, Fig. 2(b) shows that the amount of quantum squeezing continues to increase as one exits the linearized regime. A Gaussian approximation in  $X_m$  may also be made to the position measurement [49], which agrees with the exact theory for all  $\mu\sigma$ , and with the linearized approximation within its range of applicability, as shown in Fig. 2.

*Nonlinear continuous position measurement.*—In addition to pulsed measurements, our scheme in Fig. 1(c) can be used for continuous position measurement, where the record of general-dyne outcomes can be used to best estimate the quantum trajectory of the mechanical motion in the presence of the nonlinearities via a stochastic master equation (SME). The SME is derived by writing the optical drive as  $|\alpha|^2 = 2kdt$ , where  $k$  describes the photon flux, and expanding Eq. (1) to first order in  $dt$  [49]. The full SME, including mechanical open-system dynamics, is

$$d\rho = -\frac{i}{\hbar}[H_0, \rho]dt + \mathcal{D}[c]\rho dt + \mathcal{D}[L]\rho dt + \sqrt{(1-\zeta^2)\eta}\mathcal{H}[c]\rho dW_{X_l} + \zeta\sqrt{\eta}\mathcal{H}[-ic]\rho dW_{P_l}, \quad (2)$$

where  $H_0/\hbar = \omega_m b^\dagger b$ ,  $\omega_m$  is the mechanical angular frequency, the superoperators are given by  $\mathcal{D}[O]\rho = O\rho O^\dagger - \frac{1}{2}\{O^\dagger O, \rho\}$  and  $\mathcal{H}[O]\rho = O\rho + \rho O^\dagger - \langle O + O^\dagger \rangle \rho$ , the measurement output operator is  $c = \sqrt{2k}f(X_m)$ , and  $L = \sqrt{(4\gamma k_b T)/(\hbar\omega_m)}X_m + i\sqrt{(\hbar\omega_m\gamma)/(4k_b T)}P_m$ , which models quantum Brownian motion [54]. Here,  $T$  is the environmental temperature,  $\gamma$  is the mechanical decay rate, and  $\eta$  is the measurement efficiency. Further, the Wiener increments for the  $X_l$  and  $P_l$  measurements obey  $dW_i dW_j = \delta_{i,j} dt$  and  $\mathbb{E}[dW_i] = 0$ , for  $i, j = X_l, P_l$ , where  $\mathbb{E}$  represents the stochastic average. The SME of Eq. (2) is valid provided the cavity can be adiabatically eliminated, which is readily achieved in the unresolved-sideband regime, and for resolved-sideband systems,  $\kappa$  must be larger than the

interaction rate [49].

For a continuous-input drive, the measurement records of the  $X_I$  and  $P_I$  homodyne detectors are  $dy_{X_I} = \langle f_R \rangle dt + dW_{X_I}/\sqrt{8\eta(1-\zeta^2)k}$  and  $dy_{P_I} = \langle f_I \rangle dt + dW_{P_I}/\sqrt{8\eta\zeta^2 k}$ , respectively [55, 56]. And, the general-dyne measurement currents are defined by  $X_I(t) = \sqrt{4k\eta(1-\zeta^2)/\tau} \int_{t-\tau}^t dy_{X_I}$  and  $P_I(t) = \sqrt{4k\eta\zeta^2/\tau} \int_{t-\tau}^t dy_{P_I}$ , where  $\tau$  is the integration time of the homodyne detectors. Here,  $1/\tau$  must be much faster than all other relevant rates, such that the SME in Eq. (2) accurately models the continuous measurement [57]. Also, at  $\mu = 0$  the measurement currents are normalized to give  $\mathbb{E}(X_I^2) - \mathbb{E}(X_I)^2 = \mathbb{E}(P_I^2) - \mathbb{E}(P_I)^2 = 1/2$ ,  $\mathbb{E}(P_I) = 0$ , and  $\mathbb{E}(X_I) = X_\alpha \sqrt{\eta(1-\zeta^2)}$ , with  $X_\alpha^2 = 4k\tau$ .

For small optical rotations ( $\mu\sigma \ll 1$ ) Eq. (2) reduces to the standard SME of linearized optomechanics as  $c = \sqrt{2k}f(X_m) \approx \sqrt{2k} + i\sqrt{2\mu^2 k}X_m$  and  $\mu^2 k$  recovers the linearized measurement rate  $2g^2/\kappa$ , where  $g$  is the linearized coupling rate [58, 59]. However, we find that a distinct Gaussian limit of Eq. (2) exists beyond linearized optomechanics for arbitrarily large optical rotations. Curiously, in this regime, the evolution of the mechanical covariance matrix is *stochastic* as the variances depend on the measurement outcomes. We thus term this new Gaussian regime of operation the *stochastic Gaussian regime*. To derive this regime, at every time step  $t \rightarrow t + dt$  we write  $\mu X_m = \mu \langle X_m \rangle + \mu Y_m$  in Eq. (2). Provided  $\text{Var}(\mu Y_m) \ll 1$ , which implies weak single-photon coupling, we then expand the SME to first order in  $\mu Y_m$  and the small optical phase shifts  $\mu Y_m$  may be integrated to obtain arbitrarily large optical rotations over a finite duration. Introducing  $\mathbf{r} = (Y_m, P_m)^T$ , the dynamics of the first moments  $\langle \mathbf{r} \rangle = \text{tr}(\rho \mathbf{r})$  and the covariance matrix elements  $V_{ij} = \langle \{r_i, r_j\} \rangle / 2 - \langle r_i \rangle \langle r_j \rangle$  can be computed from the Gaussian approximation to Eq. (2). In the stochastic Gaussian regime, the dynamics of an initial Gaussian mechanical state are completely described by a stochastic differential equation for  $\langle \mathbf{r} \rangle$  and a stochastic Riccati equation for  $V$

$$d\langle \mathbf{r} \rangle = (M\langle \mathbf{r} \rangle + \mathbf{d})dt + N\sqrt{\eta}d\mathbf{W}, \quad (3)$$

$$\dot{V} = MV + VM^T + D - N\eta N^T. \quad (4)$$

Here,  $\boldsymbol{\eta} = \text{diag}(\eta, \eta, 0)$  and  $d\mathbf{W} = (dW_{X_I}, dW_{P_I}, 0)^T$ . We have also introduced the displacement vector  $\mathbf{d}$  and the drift  $M$ , diffusion  $D$ , and noise  $N$  matrices, given in the Supplemental Material [49]. See e.g. Ref. [60] for other usage of the Riccati equation. Note, Eq. (4) is stochastic as  $M$ ,  $D$ , and  $N$  depend on the mean position  $\langle X_m \rangle$ .

For a fixed drive frequency at  $\Delta = 0$ , the optical phase shift averaged over a given stochastic trajectory is positive because the radiation-pressure force causes a non-zero time-averaged mean mechanical position. Hence, to maximize the amount of light that enters the cavity, and ensure the time-averaged optical phase shift is zero, we model a lock of the pump field to the mean cavity resonance frequency using a third-order Butterworth filter with a cutoff frequency at  $0.5\omega_m$ . This locking effectively cancels the

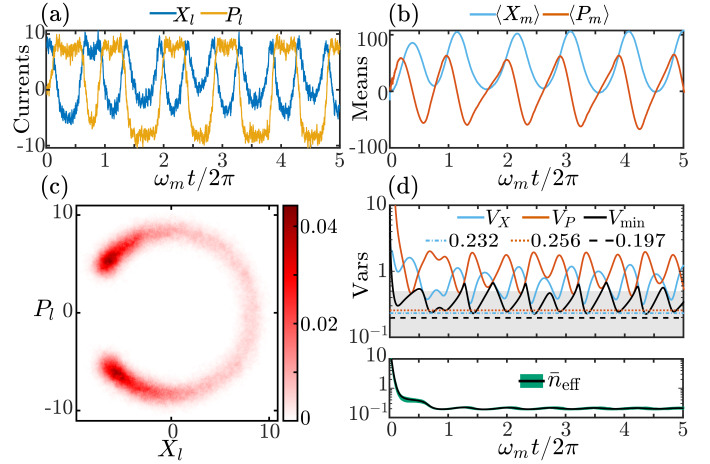


FIG. 3. Nonlinear continuous position measurement in the stochastic Gaussian regime. Here,  $X_\alpha/\sqrt{2} = 10$ ,  $\omega_m/2\pi = 10$  MHz,  $\mu = 0.05$ ,  $\mu^2 k/\omega_m = 2$ ,  $\eta = 0.7$ ,  $\gamma/2\pi = 10$  Hz,  $\zeta = 1/\sqrt{2}$ ,  $T = 4$  K ( $\bar{n} = 8.4 \times 10^3$ ), and the initial mechanical state is precooled to 100 mK ( $\bar{n} = 2.1 \times 10^2$ ). (a) The general-dyne measurement currents  $X_I$  and  $P_I$  plotted as a function of time for a given trajectory. (b) The corresponding trajectories of the mechanical means  $\langle X_m \rangle$  and  $\langle P_m \rangle$ . (c) The same general-dyne currents plotted as a normalized 2D histogram. (d) Top: The position variance  $V_X$ , the momentum variance  $V_P$ , and the minimum eigenvalue  $V_{\min}$  for the same trajectory. Here, the dashed lines correspond to the mean of the minimum of each variance quantity over 100 trajectories and the grey shaded area indicates quantum squeezing. Bottom: The effective thermal occupation  $\bar{n}_{\text{eff}}$  averaged over 100 trajectories, where the shaded green area indicates the upper and lower quartile range.

slowly varying component of  $\langle X_m \rangle$ , while the dynamics and fluctuations of the mechanical position are still measured.

The dynamics of the mechanical Gaussian state governed by Eqs (3) and (4) are solved numerically using an Euler-Maruyama method [61]. Here, we use a parameter set (see Fig. 3 caption) based on sliced-photonic crystal structures [17, 45] and more parameter sets are explored in the Supplemental Material [49]. For this continuous measurement, we choose a beamsplitter coefficient of  $\zeta = 1/\sqrt{2}$  corresponding to heterodyne detection, which is readily implemented using a single balanced detector and a frequency-offset local oscillator. Fig. 3(a) shows the general-dyne measurement currents with time for a given stochastic trajectory, and the corresponding means  $\langle X_m \rangle$  and  $\langle P_m \rangle$  are plotted in Fig. 3(b). We see the evolution of the means is anharmonic resulting from the optomechanical nonlinearities. Meanwhile, Fig. 3(c) plots the general-dyne currents as a 2D histogram in optical phase space, which is symmetric due to the drive-locking. Fig. 3(d) shows the position variance  $V_X$ , the momentum variance  $V_P$ , and the minimum eigenvalue of the covariance matrix  $V_{\min}$  for the same trajectory and the dashed lines indicate the mean of the minimum value of these quantities over 100 runs, each lasting 100 mechanical periods. We also plot the effective thermal occupation  $\bar{n}_{\text{eff}} = \sqrt{\det(V)} - 1/2 = (1/\text{tr}(\rho^2) - 1)/2$

averaged over the 100 runs. These plots show that for the modest parameters used here, quantum squeezing below 3 dB ( $V_{\min}, V_X < 0.25$ ) and effective ground-state cooling are achievable in the stochastic Gaussian regime.

*Conclusions and Outlook.*—We introduce a framework for cavity quantum optomechanics that captures the nonlinearities of both radiation-pressure and the cavity response. As a natural first application of this framework, we study mechanical position measurement in the presence of these nonlinearities, which enables mechanical information encoded on both optical quadratures throughout the full cavity phase response of  $\pm\pi$  to be measured via optical general-dyne detection. Our scheme can be employed with back-action-evading pulsed measurements or with continuous measurements and we derive a measurement operator and a stochastic master equation for each mode of operation, respectively. As well as recovering the linearized theory, our framework is capable of describing the three regimes where the linearized approximation fails: (i) the weak single-photon coupling regime but with significant optical rotations, (ii) the strong single-photon coupling regime, and (iii) systems operating at low light levels. Thus, this treatment vastly extends the range that cavity optomechanical position measurement can be performed and enables the identification of new regimes of operation, such as the stochastic Gaussian regime we identify and term here. In addition to describing how to perform mechanical quantum squeezing by measurement in nonlinear systems, our formalism will also lead to a broad range of experimental and theoretical advances in sensing, mechanical quantum state engineering, and quantum measurement and control.

*Acknowledgements.*—We acknowledge useful discussions with G. A. Brawley, R. Clarke, G.ENZIAN, L. A. Kanari-Naish, G. J. Milburn, B. A. Stickler, and S. Qvarfort. This project was supported by the Engineering and Physical Sciences Research Council (EP/T031271/1), UK Research and Innovation (MR/S032924/1), the Royal Society, and the European Research Council (ERC Starting Grant No. 759644-TOPP). This work is part of the research programme of the Netherlands Organisation for Scientific Research (NWO) and supported by an NWO Vidi grant.

---

\* [jack.clarke@imperial.ac.uk](mailto:jack.clarke@imperial.ac.uk)

† [m.vanner@imperial.ac.uk](mailto:m.vanner@imperial.ac.uk); [www.qmeas.net](http://www.qmeas.net)

- [1] A. Kronwald and F. Marquardt, *Phys. Rev. Lett.* **111**, 133601 (2013).
- [2] K. Børkje, A. Nunnenkamp, J. D. Teufel, and S. M. Girvin, *Phys. Rev. Lett.* **111**, 053603 (2013).
- [3] M. A. Lemonde, N. Didier, and A. A. Clerk, *Phys. Rev. Lett.* **111**, 053602 (2013).
- [4] M. R. Vanner, *Phys. Rev. X* **1**, 021011 (2011).
- [5] S. Bose, K. Jacobs, and P. L. Knight, *Phys. Rev. A* **59**, 3204 (1999).
- [6] M. Ringbauer, T. J. Weinhold, L. A. Howard, A. G. White, and M. R. Vanner, *New J. Phys.* **20**, 053042 (2018).
- [7] J. Clarke and M. R. Vanner, *Quantum Sci. Technol.* **4**, 014003 (2019).
- [8] W. Marshall, C. Simon, R. Penrose, and D. Bouwmeester, *Phys. Rev. Lett.* **91**, 130401 (2003).
- [9] G. Vacanti, M. Paternostro, G. M. Palma, and V. Vedral, *New J. Phys.* **10**, 095014 (2008).
- [10] U. Akram, W. P. Bowen, and G. J. Milburn, *New J. Phys.* **15**, 093007 (2013).
- [11] L. A. Kanari-Naish, J. Clarke, S. Qvarfort, and M. R. Vanner, *Quantum Sci. Technol.* **7**, 035012 (2022).
- [12] P. Rabl, *Phys. Rev. Lett.* **107**, 063601 (2011).
- [13] A. Nunnenkamp, K. Børkje, and S. M. Girvin, *Phys. Rev. Lett.* **107**, 063602 (2011).
- [14] F. Brennecke, S. Ritter, T. Donner, and T. Esslinger, *Science* **322**, 235 (2008).
- [15] T. P. Purdy, D. W. C. Brooks, T. Botter, N. Brahms, Z.-Y. Ma, and D. M. Stamper-Kurn, *Phys. Rev. Lett.* **105**, 133602 (2010).
- [16] G. A. Brawley, M. R. Vanner, P. E. Larsen, S. Schmid, A. Boisen, and W. P. Bowen, *Nat. Commun.* **7**, 10988 (2016).
- [17] R. Leijssen, G. R. La Gala, L. Freisem, J. T. Muhonen, and E. Verhagen, *Nat. Commun.* **8**, 16024 (2017).
- [18] S. A. Fedorov, A. Beccari, A. Arabmoheghi, D. J. Wilson, N. J. Engelsens, and T. J. Kippenberg, *Optica* **7**, 1609 (2020).
- [19] A. G. Krause, M. Winger, T. D. Blasius, Q. Lin, and O. Painter, *Nat. Photonics* **6**, 768 (2012).
- [20] F. Guzmán Cervantes, L. Kumanchik, J. Pratt, and J. M. Taylor, *Appl. Phys. Lett.* **104**, 221111 (2014).
- [21] J. Chaste, A. Eichler, J. Moser, G. Ceballos, R. Rurali, and A. Bachtold, *Nat. Nanotechnol.* **7**, 301 (2012).
- [22] G. Ranjit, M. Cunningham, K. Casey, and A. A. Geraci, *Phys. Rev. A* **93**, 053801 (2016).
- [23] D. Rugar, R. Budakian, H. J. Mamin, and B. W. Chui, *Nature* **430**, 329 (2004).
- [24] G. Longo, L. Alonso-Sarduy, L. M. Rio, A. Bizzini, A. Trampuz, J. Notz, G. Dietler, and S. Kasas, *Nat. Nanotechnol.* **8**, 522 (2013).
- [25] B. P. Abbott, R. Abbott, T. D. Abbott, M. R. Abernathy, F. Acernese, K. Ackley, C. Adams, T. Adams, P. Addesso, R. Adhikari, *et al.*, *Phys. Rev. Lett.* **116**, 061102 (2016).
- [26] D. C. Moore and A. A. Geraci, *Quantum Sci. Technol.* **6**, 014008 (2021).
- [27] D. Carney, G. Krnjaic, D. C. Moore, C. A. Regal, G. Afek, S. Bhave, B. Brubaker, T. Corbitt, J. Cripe, N. Crisosto, *et al.*, *Quantum Sci. Technol.* **6**, 024002 (2021).
- [28] A. A. Geraci, S. J. Smullin, D. M. Weld, J. Chiaverini, and A. Kapitulnik, *Phys. Rev. D* **78**, 022002 (2008).
- [29] V. B. Braginsky and F. Y. Khalili, *Quantum Measurement* (Cambridge University Press, 1995).
- [30] K. W. Murch, K. L. Moore, S. Gupta, and D. M. Stamper-Kurn, *Nat. Phys.* **4**, 561 (2008).
- [31] T. P. Purdy, R. W. Peterson, and C. A. Regal, *Science* **339**, 801 (2013).
- [32] J. Cripe, N. Aggarwal, R. Lanza, A. Libson, R. Singh, P. Heu, D. Follman, G. D. Cole, N. Mavalvala, and T. Corbitt, *Nature* **568**, 364 (2019).
- [33] A. C. Doherty and K. Jacobs, *Phys. Rev. A* **60**, 2700 (1999).
- [34] S. Mancini, D. Vitali, and P. Tombesi, *Phys. Rev. Lett.* **80**, 688 (1998).
- [35] P. F. Cohadon, A. Heidmann, and M. Pinard, *Phys. Rev. Lett.* **83**, 3174 (1999).
- [36] D. J. Wilson, V. Sudhir, N. Piro, R. Schilling, A. Ghadimi,

- and T. J. Kippenberg, *Nature* **524**, 325 (2015).
- [37] M. Rossi, D. Mason, J. Chen, Y. Tsaturyan, and A. Schliesser, *Nature* **563**, 53 (2018).
- [38] V. B. Braginsky, Y. I. Vorontsov, and K. S. Thorne, *Science* **209**, 547 (1980).
- [39] A. A. Clerk, F. Marquardt, and K. Jacobs, *New J. Phys.* **10**, 095010 (2008).
- [40] J. Suh, A. J. Weinstein, C. U. Lei, E. E. Wollman, S. K. Steinke, P. Meystre, A. A. Clerk, and K. C. Schwab, *Science* **344**, 1262 (2014).
- [41] I. Shomroni, L. Qiu, D. Malz, A. Nunnenkamp, and T. J. Kippenberg, *Nat. Commun.* **10**, 2086 (2019).
- [42] V. B. Braginsky, Y. I. Vorontsov, and F. Y. Khalili, *JETP Lett.* **27** (1978).
- [43] M. R. Vanner, I. Pikovski, G. D. Cole, M. S. Kim, Č. Brukner, K. Hammerer, G. J. Milburn, and M. Aspelmeyer, *Proc. Natl. Acad. Sci.* **108**, 16182 (2011).
- [44] M. R. Vanner, J. Hofer, G. D. Cole, and M. Aspelmeyer, *Nat. Commun.* **4**, 2295 (2013).
- [45] J. T. Muhonen, G. R. La Gala, R. Leijssen, and E. Verhagen, *Phys. Rev. Lett.* **123**, 113601 (2019).
- [46] N. Walker and J. E. Carroll, *Opt. Quantum Electron.* **18**, 355 (1986).
- [47] A. Furusawa, J. L. Sørensen, S. L. Braunstein, C. A. Fuchs, H. J. Kimble, and E. S. Polzik, *Science* **282**, 706 (1998).
- [48] M. D. Vidrighin, G. Donati, M. G. Genoni, X.-M. Jin, W. S. Kolthammer, M. S. Kim, A. Datta, M. Barbieri, and I. A. Walmsley, *Nat. Commun.* **5**, 3532 (2014).
- [49] See the Supplemental Material for further theoretical details and an animation of the optical Husimi- $Q$  function.
- [50] I. Pikovski, M. R. Vanner, M. Aspelmeyer, M. S. Kim, and Č. Brukner, *Nat. Phys.* **8**, 393 (2012).
- [51] Z. Wang and A. H. Safavi-Naeini, *Nat. Commun.* **8**, 15886 (2017).
- [52] U. Leonhardt, *Measuring the Quantum State of Light* (Cambridge University Press, 1997).
- [53] Note that an outcome window may be utilized to further reduce the variance at the cost of introducing a finite window-dependent heralding probability.
- [54] M. A. Schlosshauer, *Decoherence: and the Quantum-to-Classical Transition* (Springer Science & Business Media, 2007).
- [55] K. Jacobs and D. A. Steck, *Contemp. Phys.* **47**, 279 (2006); K. Jacobs, *Quantum measurement theory and its applications* (Cambridge University Press, 2014).
- [56] H. M. Wiseman and G. J. Milburn, *Quantum Measurement and Control* (Cambridge University Press, 2009).
- [57] C. M. Caves and G. J. Milburn, *Phys. Rev. A* **36**, 5543 (1987).
- [58] M. Rossi, D. Mason, J. Chen, and A. Schliesser, *Phys. Rev. Lett.* **123**, 163601 (2019).
- [59] C. Meng, G. A. Brawley, J. S. Bennett, M. R. Vanner, and W. P. Bowen, *Phys. Rev. Lett.* **125**, 043604 (2020).
- [60] J. Zhang and K. Mølmer, *Phys. Rev. A* **96**, 062131 (2017).
- [61] K. Jacobs, *Stochastic Processes for Physicists: Understanding Noisy Systems* (Cambridge University Press, 2010).

# Cavity quantum optomechanical nonlinearities and position measurement beyond the breakdown of the linearized approximation: Supplemental Material

J. Clarke<sup>1</sup>, P. Neveu<sup>2</sup>, K. E. Khosla<sup>1</sup>, E. Verhagen<sup>2</sup>, and M. R. Vanner<sup>1</sup>

<sup>1</sup>*QOLS, Blackett Laboratory, Imperial College London, London SW7 2BW, United Kingdom*  
<sup>2</sup>*Center for Nanophotonics, AMOLF, Science Park 104, 1098 XG Amsterdam, The Netherlands*

Here, we provide further details on our nonlinear theoretical framework of cavity quantum optomechanics and approach for position measurement in the nonlinear regime. Firstly, we give a step-by-step derivation of the nonlinear optomechanical unitary, the measurement operator, and the SME. Following this, we detail the calculations that show how these tools may be used to achieve pulsed and continuous measurements of mechanical position in the nonlinear regime via optical general-dyne detection. We describe the Gaussian approximation for pulsed operation and show how the equations for the stochastic Gaussian regime may be derived from the SME. Finally, we study more parameter sets based on current state-of-the-art sliced-photonic crystal devices.

## Contents

<p>I. Nonlinear cavity-enhanced unitary ..... i</p> <p style="padding-left: 20px;">A. Pulsed interaction ..... i</p> <p style="padding-left: 20px;">B. Continuous infinitesimal unitary ..... ii</p> <p>II. Measurement operator ..... iv</p> <p>III. Stochastic master equation ..... iv</p> <p style="padding-left: 20px;">A. Infinitesimal measurement operator in a rotating frame ..... iv</p> <p style="padding-left: 20px;">B. Stochastic master equation in a rotating frame ... v</p> <p style="padding-left: 20px;">C. Stochastic master equation in the lab frame ..... vi</p> <p>IV. Pulsed measurement ..... vii</p> <p style="padding-left: 20px;">A. Krauss map and heralding probability ..... vii</p> <p style="padding-left: 20px;">B. The Husimi-<math>Q</math> function and <math>\pi</math>-phase limit ..... vii</p>	<p style="padding-left: 20px;">C. Gaussian approximation to pulsed measurement . ix</p> <p style="padding-left: 20px;">D. Optical loss ..... x</p> <p style="padding-left: 20px;">E. Phase quadrature measurements ..... xi</p> <p style="padding-left: 20px;">F. Dependence on the detuning ..... xii</p> <p>V. Continuous measurement ..... xiii</p> <p style="padding-left: 20px;">A. Agreement with the linearized regime of optomechanics and the linearized measurement rate xiii</p> <p style="padding-left: 20px;">B. Stochastic Gaussian measurement regime ..... xiii</p> <p style="padding-left: 20px;">C. Drive-locking ..... xv</p> <p style="padding-left: 20px;">D. Experimental parameters for sliced-photonic crystal devices ..... xvi</p>
--	--

## I. NONLINEAR CAVITY-ENHANCED UNITARY

### A. Pulsed interaction

In the unresolved sideband regime ( $\kappa \gg \omega_m$ ), which is used for pulsed optomechanics, the Heisenberg-Langevin equations describing the dynamics generated by  $H/\hbar = -\Delta a^\dagger a - g_0 a^\dagger a (b + b^\dagger)$  are

$$\dot{a} = i(\sqrt{2}g_0 X_m + \Delta)a - \kappa a + \sqrt{2\kappa} a_{in} \quad (\text{S1})$$

$$\dot{X}_m = 0 \quad (\text{S2})$$

$$\dot{P}_m = \sqrt{2}g_0 a^\dagger a, \quad (\text{S3})$$

for an input pulse at  $\omega_l$  in a frame rotating at the cavity frequency  $\omega_c$ . Here, the detuning is  $\Delta = \omega_l - \omega_c$  and we neglect free mechanical evolution and dissipation as the interaction time is much less than the mechanical period. The operator  $a_{in}(t)$  describes the time-dependent input to the cavity mode and  $X_m = (b + b^\dagger)/\sqrt{2}$ . Furthermore, in pulsed optomechanics the cavity field can be adiabatically eliminated  $\dot{a} = 0$  if  $\kappa \gg \tau_{in}^{-1}$ , where  $\tau_{in}$  is the characteristic timescale over which the input  $a_{in}$  changes. In these limits, the equations of motions may be solved to obtain

$$a(t) = \sqrt{2\kappa} \int_{-\infty}^t dt' a_{in}(t') e^{-[\kappa - i(\sqrt{2}g_0 X_m + \Delta)]|t-t'|}. \quad (\text{S4})$$

Generally, if  $h(t')$  is a slowly varying function, such that  $\kappa \gg \tau_h^{-1}$ , where  $\tau_h$  is the characteristic timescale over which the function  $h(t')$  changes,

$$\begin{aligned} h(t') e^{-\kappa|t-t'|} &\simeq h(t') \frac{2}{\kappa} \delta(t-t') \\ &= h(t) \frac{2}{\kappa} \delta(t-t') \\ &\simeq h(t) e^{-\kappa|t-t'|}. \end{aligned} \quad (\text{S5})$$

Here, we used that  $\lim_{\kappa \rightarrow \infty} \frac{\kappa}{2} e^{-\kappa|t-t'|} = \delta(t-t')$ . This property (S5) implies that  $a_{in}(t')e^{-[\kappa-i(\sqrt{2}g_0X_m+\Delta)]|t-t'|} = a_{in}(t)e^{-[\kappa-i(\sqrt{2}g_0X_m+\Delta)]|t-t'|}$  if  $\kappa \gg \tau_{in}^{-1}$ , regardless of  $g_0$ ,  $X_m$ , and  $\Delta$ , which contribute only to the phase term. The expression for  $a(t)$  in Eq. (S4) then becomes

$$\begin{aligned} a(t) &= \sqrt{2\kappa}a_{in}(t) \int_{-\infty}^t dt' e^{-[\kappa-i(\sqrt{2}g_0X_m+\Delta)](t-t')} \\ &= \frac{\sqrt{2\kappa}}{\kappa - i(\sqrt{2}g_0X_m + \Delta)} a_{in}(t), \end{aligned} \quad (\text{S6})$$

which amounts to adiabatic elimination of the cavity field  $\dot{a} = 0$  in Eq. (S1).

Using the input-output relations for the cavity  $a_{out}(t) = \sqrt{2\kappa}a(t) - a_{in}(t)$ , and defining the nonlinear optomechanical coupling strength  $\mu = \sqrt{8}g_0/\kappa$ , then gives

$$a_{out}(t) = \frac{1 + i\left(\frac{\mu}{2}X_m + \frac{\Delta}{\kappa}\right)}{1 - i\left(\frac{\mu}{2}X_m + \frac{\Delta}{\kappa}\right)} a_{in}(t). \quad (\text{S7})$$

While defining the photon number operator  $n_l$  to be

$$n_l = \int_0^{\tau_p} a_{in}^\dagger a_{in}(t) dt = \int_0^{\tau_p} a_{out}^\dagger a_{out}(t) dt, \quad (\text{S8})$$

allows us to integrate Eq. (S3), and using (S6), we arrive at

$$P_m(\tau_p) - P_m(0) = \frac{\mu}{1 + \left(\frac{\mu}{2}X_m + \frac{\Delta}{\kappa}\right)^2} n_l, \quad (\text{S9})$$

where  $\tau_p$  is the duration of the pulsed optomechanical interaction.

Introducing the nonlinear response function  $f(X_m) = [1 + i\left(\frac{\mu}{2}X_m + \frac{\Delta}{\kappa}\right)] / [1 - i\left(\frac{\mu}{2}X_m + \frac{\Delta}{\kappa}\right)]$  and the nonlinear phase  $\varphi(X_m) = \arg(f)$ , allows us to write Eqs (S7) and (S9) as

$$a_{out} = f(X_m)a_{in}, \quad (\text{S10})$$

$$P_m(\tau_p) = P_m(0) + \frac{\partial\varphi(X_m)}{\partial X_m} n_l, \quad (\text{S11})$$

which are equivalent to Heisenberg transformations

$$a_{out} = U^\dagger a_{in} U, \quad (\text{S12})$$

$$P_m(\tau_p) = U^\dagger P_m(0) U, \quad (\text{S13})$$

with the nonlinear pulsed optomechanical unitary given by  $U = e^{i\varphi(X_m)n_l}$ . The equivalence between Eqs (S10) and (S12), may be understood via the equation for phase-space rotations  $a_{out} = e^{i\phi n_l} a_{in} e^{-i\phi n_l} = (\cos\phi - i\sin\phi) a_{in}$ . Furthermore, the Hadamard lemma

$$e^X Y e^{-X} = Y + [X, Y] + \frac{1}{2!} [X, [X, Y]] + \dots + \frac{1}{n!} [X, [X, \dots, [X, Y] \dots]] + \dots,$$

along with  $[\varphi(X_m), P_m] = i\frac{\partial\varphi(X_m)}{\partial X_m}$ , can be used to derive the equivalence between Eqs (S11) and (S13).

When  $\Delta = 0$ , expanding  $U = e^{i\varphi(X_m)n_l}$  to second order in  $X_m$  agrees with the nonlinear unitary  $e^{i\mu X_m n_l}$  of [I. Pikovski *et al.*, Nat. Phys. **8**, 393 (2012); Z. Wang and A. H. Safavi-Naeini, Nat. Commun. **8**, 1 (2017)]. The higher orders in  $X_m$  account for the nonlinearity of the cavity response. Furthermore, the linearized unitary is recovered in the limit of small optical rotations and large intracavity amplitude:  $a \rightarrow \alpha_c + \delta a$  and  $|\alpha_c| \gg \langle |\delta a| \rangle$  [M. R. Vanner *et al.*, Proc. Natl. Acad. Sci. **108**, 16182 (2011)]. Finally, we note that for our single cavity mode treatment to be valid the change in the cavity frequency due to a displacement  $X_m$ , which for  $\Delta = 0$  is  $|\omega_c(X_m) - \omega_c| = \sqrt{2}g_0X_m \simeq \sqrt{2}g_0\sigma$ , must be much smaller than the distance in frequency space to the next optical mode  $\omega_{fsr}$ . This condition ensures neighbouring cavity modes can be ignored and division by  $\kappa$  allows one to write this condition as  $\mu\sigma \ll 2\mathcal{F}_c$ , where  $\mathcal{F}_c = \omega_{fsr}/\kappa$  is the cavity finesse.

## B. Continuous infinitesimal unitary

The optomechanical Hamiltonian is  $H_{om} = \hbar\omega_c a^\dagger a + \hbar\omega_m b^\dagger b - \hbar g_0 a^\dagger a (b + b^\dagger) = H_0 + H$ , with  $H_0 = \hbar\omega_c a^\dagger a + \hbar\omega_m b^\dagger b$  and  $H = -\hbar g_0 a^\dagger a (b + b^\dagger)$ . Transforming from the lab frame to a rotating frame using  $\tilde{H} = U_F^\dagger H_{om} U_F + i\hbar \dot{U}_F^\dagger U_F$ , with



$U_F = e^{-i\omega_m a^\dagger a t - i\omega_m b^\dagger b t}$  gives

$$\begin{aligned}\tilde{H}/\hbar &= -\Delta a^\dagger a - g_0 a^\dagger a (b e^{-i\omega_m t} + b^\dagger e^{+i\omega_m t}), \\ &= -\Delta a^\dagger a - \sqrt{2} g_0 a^\dagger a \tilde{X}_m,\end{aligned}\tag{S14}$$

$$\tag{S15}$$

where  $\tilde{X}_m = X_m \cos \omega_m t + P_m \sin \omega_m t$  and  $\tilde{P}_m = P_m \cos \omega_m t - X_m \sin \omega_m t$ . In this rotating frame, the Heisenberg-Langevin equations with optical driving of the cavity are given by

$$\dot{\tilde{X}}_m = -\sqrt{2} g_0 a^\dagger a \sin \omega_m t,\tag{S16}$$

$$\dot{\tilde{P}}_m = \sqrt{2} g_0 a^\dagger a \cos \omega_m t,\tag{S17}$$

$$\dot{a} = i \left[ \sqrt{2} g_0 (X_m \cos \omega_m t + P_m \sin \omega_m t) + \Delta \right] a - \kappa a + \sqrt{2} \kappa a_{in}\tag{S18}$$

We have not included mechanical interactions with the bath as they aren't a part of the construction of the infinitesimal unitary. These mechanics-bath interactions will be included in the SME via a Lindblad dissipator. Solving these equations over an arbitrary infinitesimal time window  $t \rightarrow t + dt$  gives

$$X_m(t + dt) = X_m(t) - \sqrt{2} g_0 a^\dagger a \sin(\omega_m t) dt,\tag{S19}$$

$$P_m(t + dt) = P_m(t) + \sqrt{2} g_0 a^\dagger a \cos(\omega_m t) dt,\tag{S20}$$

$$a(t + dt) = a(t) + i \left( \sqrt{2} g_0 \tilde{X}_m + \Delta \right) a dt - \kappa a dt + \sqrt{2} \kappa a_{in} dt.\tag{S21}$$

We now consider a ‘good position measurement’ where the cavity field adiabatically follows the mechanical oscillator [A. C. Doherty and K. Jacobs, *Phys. Rev. A* **60**, 2700 (1999)]. Such a measurement is readily achieved in the unresolved sideband regime  $\kappa \gg \omega_m$ , as the cavity field responds quickly to the mechanical motion and adiabatically follows the mechanical oscillator [G. Brawley, *et al.*, *Nat. Commun.* **7**, 10988 (2016)]. Outside the unresolved sideband regime, adiabatic elimination of the cavity mode is also valid, provided the cavity decay rate exceeds other rates in the Hamiltonian [H. M. Wiseman and G. J. Milburn, *Phys. Rev. A* **47**, 642 (1993)].

In the adiabatic regime, the cavity field rapidly reaches the steady state  $\dot{a} = 0$  on the order of  $1/\kappa$  and so together with Eq. (S21), the cavity input-output relation gives

$$a_{out}(t) = \frac{1 + i \left( \frac{\mu}{2} \tilde{X}_m(t) + \frac{\Delta}{\kappa} \right)}{1 - i \left( \frac{\mu}{2} \tilde{X}_m(t) + \frac{\Delta}{\kappa} \right)} a_{in}(t).\tag{S22}$$

The definition of the photon number operator in Eq. (S8) implies that over a time increment  $dt$ ,  $n_l(dt) = a_{in}^\dagger a_{in} dt$ , and therefore

$$X_m(t + dt) = X_m(t) - \frac{\mu}{1 + \left( \frac{\mu}{2} \tilde{X}_m + \frac{\Delta}{\kappa} \right)^2} \sin(\omega_m t) n_l(dt),\tag{S23}$$

$$P_m(t + dt) = P_m(t) + \frac{\mu}{1 + \left( \frac{\mu}{2} \tilde{X}_m + \frac{\Delta}{\kappa} \right)^2} \cos(\omega_m t) n_l(dt).\tag{S24}$$

We make an ansatz for the infinitesimal unitary in this interaction picture to be  $U_I(dt) = e^{i\varphi(\tilde{X}_m)n_l(dt)}$ . Here, we explicitly labelled the dependence on  $dt$ . Similarly to the derivation of the pulsed nonlinear unitary, this ansatz can be shown to give the same expression as Eqs (S22), (S23) and (S24) through

$$a_{out}(t) = U_I^\dagger(dt) a_{in}(t) U_I(dt),\tag{S25}$$

$$X_m(t + dt) = U_I^\dagger(dt) X_m(t) U_I(dt),\tag{S26}$$

$$P_m(t + dt) = U_I^\dagger(dt) P_m(t) U_I(dt).\tag{S27}$$

To derive the last two equations the Hadamard lemma was again employed and the following property was used: for a function of two the conjugate variables  $f(X_m, P_m)$ , we have  $[f(X_m, P_m), X_m] = -i \frac{\partial f}{\partial P_m}$  and  $[f(X_m, P_m), P_m] = +i \frac{\partial f}{\partial X_m}$ .

## II. MEASUREMENT OPERATOR

The nonlinear pulsed unitary  $U = e^{i\varphi(X_m)n_l}$  acts on the input coherent state  $|\alpha\rangle$  via  $U|\alpha\rangle = |\alpha(f_R(X_m) + if_I(X_m))\rangle$ , where the nonlinear response function has been decomposed into its real and imaginary parts  $f(X_m) = f_R(X_m) + if_I(X_m)$ ,

$$f_R(X_m) = \frac{1 - \left(\frac{\mu}{2}X_m + \frac{\Delta}{\kappa}\right)^2}{1 + \left(\frac{\mu}{2}X_m + \frac{\Delta}{\kappa}\right)^2}, \quad (\text{S28})$$

$$f_I(X_m) = \frac{2\left(\frac{\mu}{2}X_m + \frac{\Delta}{\kappa}\right)}{1 + \left(\frac{\mu}{2}X_m + \frac{\Delta}{\kappa}\right)^2}. \quad (\text{S29})$$

$$(\text{S30})$$

Furthermore, note that  $f_R^2 + f_I^2 = 1$  and  $\varphi(X_m) = \arg(f) = \arg(f_R + if_I)$ , so  $f_R(X_m) = \cos[\varphi(X_m)]$  and  $f_I(X_m) = \sin[\varphi(X_m)]$ , which clarifies that  $U$  rotates the initial coherent state through an angle  $\varphi(X_m)$  for a given value of  $X_m$ .

The action of the nonlinear pulsed optomechanical interaction, followed by optical general-dyne measurement is described by the measurement operator

$$\begin{aligned} \Upsilon &= \langle X_l | \langle P_l | BU |\alpha\rangle |0\rangle \\ &= \left\langle X_l \left| \sqrt{1 - \zeta^2} \alpha (f_R(X_m) + if_I(X_m)) \right. \right\rangle \langle P_l | \zeta \alpha (f_R(X_m) + if_I(X_m)) \rangle \\ &= \frac{1}{\sqrt{\pi}} \exp \left[ -\frac{1}{2} \left( X_l - \sqrt{1 - \zeta^2} X_\alpha f_R(X_m) \right)^2 - \frac{1}{2} (P_l - \zeta X_\alpha f_I(X_m))^2 - i\zeta X_\alpha P_l f_R(X_m) \right. \\ &\quad \left. + i\sqrt{1 - \zeta^2} X_\alpha X_l f_I(X_m) - \frac{i}{2} (1 - 2\zeta^2) X_\alpha^2 f_R(X_m) f_I(X_m) \right], \end{aligned} \quad (\text{S31})$$

where  $\alpha = X_\alpha/\sqrt{2}$  and  $X_\alpha$  is assumed real without loss of generality. At the output of the optomechanical cavity, the optical mode mixes with vacuum  $|0\rangle$  at a beamsplitter, described by  $B$ . While at the beamsplitter outputs, light is sent towards the phase  $P_l$  or amplitude  $X_l$  homodyne, in a proportion determined by the beamsplitter parameter  $\zeta$ . If the annihilation operator of the optical mode in the vacuum state is given by  $a_v$ , the Heisenberg transformations at the beamsplitter are given by  $B^\dagger a B = \zeta a + \sqrt{1 - \zeta^2} a_v$  and  $B^\dagger a_v B = \zeta a_v - \sqrt{1 - \zeta^2} a$ .

## III. STOCHASTIC MASTER EQUATION

### A. Infinitesimal measurement operator in a rotating frame

The infinitesimal measurement operator  $\Upsilon_I(\Delta t)$  describes the action of the continuous general-dyne measurement over a small time increment  $\Delta t$ . In the rotating frame, it is given by

$$\begin{aligned} \Upsilon_I(\Delta t) &= \langle X_l | \langle P_l | BU_I(\Delta t) |\alpha\rangle |0\rangle \\ &= \left\langle X_l \left| \sqrt{1 - \zeta^2} \alpha \left( f_R(\tilde{X}_m) + if_I(\tilde{X}_m) \right) \right. \right\rangle \left\langle P_l \left| \zeta \alpha \left( f_R(\tilde{X}_m) + if_I(\tilde{X}_m) \right) \right. \right\rangle \\ &= \Upsilon_I(X_l) \Upsilon_I(P_l), \end{aligned} \quad (\text{S32})$$

$$\Upsilon_I(X_l) = \frac{1}{\pi^{1/4}} \exp \left[ -\frac{a_\alpha^2}{2} \left( f_R(\tilde{X}_m) - \frac{X_l}{a_\alpha} \right)^2 + ia_\alpha^2 \frac{X_l}{a_\alpha} f_I(\tilde{X}_m) - \frac{i}{2} a_\alpha^2 f_R(\tilde{X}_m) f_I(\tilde{X}_m) \right], \quad (\text{S33})$$

$$\Upsilon_I(P_l) = \frac{1}{\pi^{1/4}} \exp \left[ -\frac{b_\alpha^2}{2} \left( f_I(\tilde{X}_m) - \frac{P_l}{b_\alpha} \right)^2 - ib_\alpha^2 \frac{P_l}{b_\alpha} f_R(\tilde{X}_m) + \frac{i}{2} b_\alpha^2 f_R(\tilde{X}_m) f_I(\tilde{X}_m) \right], \quad (\text{S34})$$

where we have split up the measurement operator into a part corresponding to the  $X_l$  measurement and the  $P_l$  measurement. We have also introduced  $a_\alpha = \sqrt{1 - \zeta^2} X_\alpha$  and  $b_\alpha = \zeta X_\alpha$ .

The  $\Delta t$  dependence in  $\Upsilon_I(\Delta t)$  comes in as the mean number of input photons in a  $\Delta t$  is  $N_p = |\alpha|^2 = \frac{1}{2} X_\alpha^2 = |\alpha_{in}|^2 \Delta t$ . Here,  $\alpha$  is the dimensionless input amplitude, which depends on  $\Delta t$ , whereas  $\alpha_{in}$  is the input field amplitude in units of  $s^{-1/2}$  and does not depend on  $\Delta t$ . For later convenience we define  $k$  to be half of the input photon flux  $k = |\alpha_{in}|^2/2$  so  $X_\alpha^2 = 4k\Delta t$ .

## B. Stochastic master equation in a rotating frame

### *A general continuous homodyne measurement*

To derive the SME for our continuous nonlinear cavity optomechanical general-dyne-based position measurement, we first consider the SME that results from a continuous homodyne measurement of the Hermitian observable  $X = X^\dagger$ . Over a time increment  $\Delta t$ , the measurement operator for such a measurement is given by the following

$$v(\Delta t) = \frac{1}{\pi^{\frac{1}{4}}} \exp \left[ -2k\Delta t(X - \bar{X})^2 + 4ik\Delta t\bar{X}Y - 2ik\Delta tXY \right], \quad (\text{S35})$$

$$\bar{X} = \langle X \rangle + \frac{1}{\sqrt{8k}} \frac{\Delta W}{\Delta t}, \quad (\text{S36})$$

$$c_v = \sqrt{2k}(X + iY). \quad (\text{S37})$$

This measurement operator is similar to the operator used in [K. Jacobs and D. A. Steck, *Contemp. Phys.* **47**, 279 (2006)] to derive continuous position measurement but with additional unitary terms that describe homodyne-measurement back action. Here,  $k$  is the measurement rate,  $\bar{X}$  is the measurement record,  $Y$  is another Hermitian operator, satisfying  $[X, Y] = 0$ , that leads to back action, and  $c_v$  will turn out to be the measurement output operator. The Wiener increment  $\Delta W$  is a Gaussian random variable with zero mean and variance  $\Delta t$ , which obeys the Itô rule  $(\Delta W)^2 = \Delta t$ . The Itô rule is strictly only true in the limit  $\Delta t \rightarrow dt$ ,  $\Delta W \rightarrow dW$ , but we will take this limit shortly in order to derive the SME.

We may write the homodyne measurement operator as  $v(\Delta t) \propto e^{-2k\Delta t[X^2 - 2\langle X \rangle(X + iY) + iXY] + \sqrt{2k}(X + iY)\Delta W}$ , ignoring terms in the exponential which are not operators and so will only effect the state normalization. Then considering an infinitesimal change in the state  $|\psi(t + dt)\rangle = |\psi(t)\rangle + d|\psi\rangle = \mathcal{N} \lim_{\Delta t \rightarrow dt} v(\Delta t) |\psi(t)\rangle$ , and expanding to first order in  $\Delta t$  with the Itô rule, gives

$$\begin{aligned} |\psi(t + dt)\rangle &= |\psi(t)\rangle + d|\psi\rangle \\ &= \lim_{\Delta t \rightarrow dt} \mathcal{N} \left\{ 1 - k\Delta t[X^2 + Y^2 - 4\langle X \rangle(X + iY)] + \sqrt{2k}(X + iY)\Delta W \right\} |\psi(t)\rangle. \end{aligned} \quad (\text{S38})$$

Here, the normalization of the state is given by  $\mathcal{N} = 1 - k\Delta t \langle X \rangle^2 - \sqrt{2k} \langle X \rangle \Delta W$ . This leads to the stochastic Schrödinger equation for a general continuous homodyne measurement

$$d|\psi\rangle = \left\{ -k[(X - \langle X \rangle)^2 + Y^2 - 2i\langle X \rangle Y]dt + \sqrt{2k}[X - \langle X \rangle + iY]dW \right\} |\psi\rangle. \quad (\text{S39})$$

Following the derivation in [K. Jacobs and D. A. Steck, *Contemp. Phys.* **47**, 279 (2006)], we may use  $d\rho = d|\psi\rangle\langle\psi| + |\psi\rangle d\langle\psi| + d|\psi\rangle d\langle\psi|$  to derive the SME for general homodyne measurement

$$\begin{aligned} d\rho &= -k[X^2\rho + \rho X^2 - 2X\rho X + Y^2\rho + \rho Y^2 - 2Y\rho Y - 2iY\rho X + 2iX\rho Y]dt + \sqrt{2k}[(X + iY)\rho + \rho(X - iY) - 2\langle X \rangle\rho]dW, \\ &= \mathcal{D}[c_v]\rho dt + \mathcal{H}[c_v]\rho dW. \end{aligned} \quad (\text{S40})$$

Here, we see that  $c_v$  is the measurement output operator. The first term in Eq. (S40) represents measurement back action and the Lindblad superoperator is given by  $\mathcal{D}[O]\rho = O\rho O^\dagger - \frac{1}{2}\{O^\dagger O, \rho\}$ . Furthermore, the second term in Eq. (S40) describes localization of  $X$ , with the measurement superoperator being  $\mathcal{H}[O]\rho = O\rho + \rho O^\dagger - \langle O + O^\dagger \rangle \rho$ .

### *Continuous general-dyne measurement*

Writing out the individual homodyne measurement operators  $\Upsilon_I(X_l)$  and  $\Upsilon_I(P_l)$  in the form of Eqs (S35), (S36), and (S37) gives

$$\Upsilon_I(X_l) = \frac{1}{\pi^{\frac{1}{4}}} \exp \left[ -\frac{a_\alpha^2}{2}(f_R(\tilde{X}_m) - \frac{X_l}{a_\alpha})^2 + ia_\alpha^2 \frac{X_l}{a_\alpha} f_I(\tilde{X}_m) - \frac{i}{2} a_\alpha^2 f_R(\tilde{X}_m) f_I(\tilde{X}_m) \right], \quad (\text{S41})$$

$$\frac{X_l}{a_\alpha} = \left\langle f_R(\tilde{X}_m) \right\rangle + \frac{1}{\sqrt{8k(1-\zeta^2)}} \frac{\Delta W_{X_l}}{\Delta t}, \quad (\text{S42})$$

$$\tilde{c}_{X_l} = \sqrt{2k(1-\zeta^2)} f(\tilde{X}_m), \quad (\text{S43})$$

and

$$\Upsilon_I(P_l) = \frac{1}{\pi^{\frac{1}{4}}} \exp \left[ -\frac{b_\alpha^2}{2} \left( f_I(\tilde{X}_m) - \frac{P_l}{b_\alpha} \right)^2 - i b_\alpha^2 \frac{P_l}{b_\alpha} f_R(\tilde{X}_m) + \frac{i}{2} b_\alpha^2 f_R(\tilde{X}_m) f_I(\tilde{X}_m) \right], \quad (\text{S44})$$

$$\frac{P_l}{b_\alpha} = \left\langle f_I(\tilde{X}_m) \right\rangle + \frac{1}{\sqrt{8k\zeta^2}} \frac{\Delta W_{P_l}}{\Delta t}, \quad (\text{S45})$$

$$\tilde{c}_{P_l} = -i\sqrt{2k\zeta^2} f(\tilde{X}_m). \quad (\text{S46})$$

Here, the  $\Delta t$  dependence comes in through  $X_\alpha^2 = 4k\Delta t$  to give  $a_\alpha^2 = 4k(1 - \zeta^2)\Delta t$  and  $b_\alpha^2 = 4k\zeta^2\Delta t$ . The Wiener increments from the two homodyne measurements are independent  $\Delta W_i \Delta W_j = \delta_{i,j} \Delta t$ .

Then using the result of Eq. (S40), we have that in the rotating frame, the continuous general-dyne measurement produces the nonlinear SME

$$d\tilde{\rho} = \mathcal{D}[\tilde{c}_{X_l}] \tilde{\rho} dt + \mathcal{D}[\tilde{c}_{P_l}] \tilde{\rho} dt + \mathcal{H}[\tilde{c}_{X_l}] \tilde{\rho} dW_{X_l} + \mathcal{H}[\tilde{c}_{P_l}] \tilde{\rho} dW_{P_l} \quad (\text{S47})$$

$$\begin{aligned} &= 2k \left( f(\tilde{X}_m) \tilde{\rho} f(-\tilde{X}_m) - \tilde{\rho} \right) dt \\ &+ \sqrt{2k(1 - \zeta^2)} \left( f(\tilde{X}_m) \tilde{\rho} + \tilde{\rho} f(-\tilde{X}_m) - 2 \left\langle f_R(\tilde{X}_m) \right\rangle \tilde{\rho} \right) dW_{X_l} \\ &+ \sqrt{2k\zeta^2} \left( -i f(\tilde{X}_m) \tilde{\rho} + i \tilde{\rho} f(-\tilde{X}_m) - 2 \left\langle f_I(\tilde{X}_m) \right\rangle \tilde{\rho} \right) dW_{P_l}, \end{aligned} \quad (\text{S48})$$

where  $\tilde{\rho}$  is the mechanical state in the rotating frame. Then introducing  $\tilde{c} = \sqrt{2k} f(\tilde{X}_m)$ ,  $\tilde{c}_{X_l} = \sqrt{1 - \zeta^2} \tilde{c}$ , and  $\tilde{c}_{P_l} = -i\zeta \tilde{c}$ , allows us to write the nonlinear SME as

$$d\tilde{\rho} = \mathcal{D}[\tilde{c}] \tilde{\rho} dt + \sqrt{1 - \zeta^2} \mathcal{H}[\tilde{c}] \tilde{\rho} dW_{X_l} + \zeta \mathcal{H}[-i\tilde{c}] \tilde{\rho} dW_{P_l}, \quad (\text{S49})$$

with  $dW_i dW_j = \delta_{i,j} dt$ ,  $\mathbb{E}[dW_i] = 0$ , for  $i, j = X_l, P_l$ . Here, the stochastic average is represented by  $\mathbb{E}$  to differentiate from the quantum expectation value.

### C. Stochastic master equation in the lab frame

The state in the lab frame is  $\rho(t) = U_F(t) \tilde{\rho}(t) U_F^\dagger(t)$ , so then

$$\begin{aligned} \rho(t + dt) &= U_F(t + dt) \tilde{\rho}(t + dt) U_F^\dagger(t + dt) \\ &= U_F(t) U_F(dt) \tilde{\rho}(t) U_F^\dagger(t) U_F^\dagger(dt) + U_F(t) d\tilde{\rho}(t) U_F^\dagger(t) \\ &= (1 - iH_0/\hbar dt) \rho(t) (1 + iH_0/\hbar dt) + U_F(t) d\tilde{\rho}(t) U_F^\dagger(t), \end{aligned} \quad (\text{S50})$$

where  $H_0 = \hbar\omega_m b^\dagger b$  is the free mechanical Hamiltonian and terms higher order than  $dt$  have been dropped. Note, the cavity part of  $H_0$  does not act on the mechanical subspace so is ignored here. Therefore, as  $\rho(t + dt) = \rho(t) + d\rho$ , we can identify

$$d\rho = -\frac{i}{\hbar} [H_0, \rho] dt + U_F(t) d\tilde{\rho}(t) U_F^\dagger(t). \quad (\text{S51})$$

by using  $U_F^\dagger U_F = \mathbf{1}$ ,  $X_m^n = U_F \tilde{X}_m^n U_F^\dagger$ , and  $c = U_F \tilde{c} U_F^\dagger = \sqrt{2k} f(X_m)$ , we have that  $U_F \mathcal{D}[\tilde{c}] \tilde{\rho} U_F^\dagger = \mathcal{D}[c] \rho$ . Then using that expectation values are the same in the rotating and the lab frame  $\langle \tilde{c} \rangle = \text{tr}(\tilde{c} \tilde{\rho}) = \text{tr}(c \rho) = \langle c \rangle$ , we have that  $U_F \mathcal{H}[\tilde{c}] \tilde{\rho} U_F^\dagger = \mathcal{H}[c] \rho$ . Hence, we find that

$$U_F(t) d\tilde{\rho}(t) U_F^\dagger(t) = \mathcal{D}[c] \rho dt + \sqrt{1 - \zeta^2} \mathcal{H}[c] \rho dW_{X_l} + \zeta \mathcal{H}[-ic] \rho dW_{P_l}, \quad (\text{S52})$$

which shows that the nonlinear SME for an ideal continuous optomechanical general-dyne position measurement is

$$d\rho = -\frac{i}{\hbar} [H_0, \rho] dt + \mathcal{D}[c] \rho dt + \sqrt{1 - \zeta^2} \mathcal{H}[c] \rho dW_{X_l} + \zeta \mathcal{H}[-ic] \rho dW_{P_l}. \quad (\text{S53})$$

#### *Mechanical dissipation, inefficient detection and the total stochastic master equation*

Inefficient detection is accounted for by the transformation  $\mathcal{H}[O] \rightarrow \sqrt{\eta} \mathcal{H}[O]$ , where  $\eta$  is the detection efficiency [H. M. Wiseman and G. J. Milburn, *Quantum measurement and control* (Cambridge university press, 2009)]. In general,

the efficiencies of the  $P_l$  and  $X_l$  homodyne measurement may be different, so we label these efficiencies  $\eta_{X_l}$  and  $\eta_{P_l}$ , respectively. While mechanical interactions with the environment may be accounted for with an additional Lindblad dissipator  $L = \sqrt{\frac{4\gamma k_b T}{\hbar\omega_m}} X_m + i\sqrt{\frac{\hbar\omega_m\gamma}{4k_b T}} P_m$ , which models quantum Brownian motion [M. A. Schlosshauer, *Decoherence: and the quantum-to-classical transition* (Springer Science & Business Media, 2007)]. Here,  $T$  is the effective temperature of the environment and  $\gamma$  is the mechanical decay rate. To summarize, the total SME for our general-dyne measurement is

$$d\rho = -\frac{i}{\hbar}[H_0, \rho]dt + \mathcal{D}[c]\rho dt + \mathcal{D}[L]\rho dt + \sqrt{(1-\zeta^2)\eta_{X_l}}\mathcal{H}[c]\rho dW_{X_l} + \zeta\sqrt{\eta_{P_l}}\mathcal{H}[-ic]\rho dW_{P_l}. \quad (\text{S54})$$

#### IV. PULSED MEASUREMENT

For a pulsed optomechanical measurement we will consider the case of a resonant input pulse  $\Delta = 0$  as we also assume an initial mechanical state with  $\langle X_m \rangle = 0$ , this setting maximizes the amount of light that can enter the cavity.

##### A. Krauss map and heralding probability

The action of a nonlinear pulsed measurement on an initial mechanical state  $\rho_i$  is described by the Krauss map

$$\rho_f = \frac{\Upsilon\rho_i\Upsilon^\dagger}{\mathcal{P}}, \quad (\text{S55})$$

where  $\Upsilon$  is given by Eq. (S31),  $\rho_f$  is the mechanical state after the measurement, and  $\mathcal{P} = \text{tr}(\Upsilon^\dagger\Upsilon\rho_i)$  is the heralding probability for a particular  $(X_l, P_l)$  general-dyne outcome. Eq. (S55) implies that the position probability changes according to  $P_f(X_m) = F(X_m)P_i(X_m)/\mathcal{P}$ , where  $P_i(X_m) = \langle X_m | \rho_i | X_m \rangle$ ,  $P_f(X_m) = \langle X_m | \rho_f | X_m \rangle$ , and as  $[\Upsilon, X_m] = 0$  implies  $\Upsilon | X_m \rangle = | X_m \rangle \Upsilon(X_m)$ , the filtering function may be written as  $F(X_m) = \Upsilon^\dagger(X_m)\Upsilon(X_m)$ , which filters the initial probability distribution to produce the final mechanical position probability. Explicitly, the filtering function is

$$F = \frac{1}{\pi} \exp [-(X_l - a_\alpha f_R(X_m))^2 - (P_l - b_\alpha f_I(X_m))^2], \quad (\text{S56})$$

where  $f_R$  and  $f_I$  are now functions of the variable  $X_m$  and are not operators.

##### B. The Husimi-Q function and $\pi$ -phase limit

*Mathematical expression for the Husimi-Q function*

The Husimi-Q function of the reduced state of the optical mode  $\rho_l$  after the optomechanical interaction is  $Q(\beta) = \frac{1}{2\pi} \langle \beta | \rho_l | \beta \rangle$ , where  $\rho_l = \text{tr}_m(U |\alpha\rangle \langle \alpha| \rho_i U^\dagger)$ . Therefore

$$\begin{aligned} Q(\beta) &= \frac{1}{2\pi} \int dX_m P_i(X_m) |\langle \beta | \alpha(f_R + if_I) \rangle|^2 \\ &= \frac{1}{2\pi} \int dX_m P_i(X_m) e^{-|\beta - \alpha(f_R + if_I)|^2}. \end{aligned} \quad (\text{S57})$$

Then writing the complex amplitudes as  $\alpha(f_R + if_I) = X_\alpha(f_R + if_I)/\sqrt{2}$  and  $\beta = (X_\beta + iP_\beta)/\sqrt{2}$  gives

$$Q(X_\beta, P_\beta) = \frac{1}{2\pi} \int dX_m P_i(X_m) e^{-\frac{1}{2}(X_\beta - X_\alpha f_R)^2 - \frac{1}{2}(P_\beta - X_\alpha f_I)^2}. \quad (\text{S58})$$

Fig. S1 shows the  $Q$  functions of the optical state after the optomechanical interactions and compares the results of this work with that induced by the unitary  $e^{i\mu X_m n_l}$ , which does not include the nonlinearity of the cavity response, demonstrating the nonlinear optomechanical phase shift. Here, we give  $\mu\sigma$  in multiples of  $\pi$  as when  $e^{i\mu X_m n_l}$  is valid,  $\mu X_m$  is the optical phase and so  $\mu\sigma$  represents a standard deviation in the optical phase.

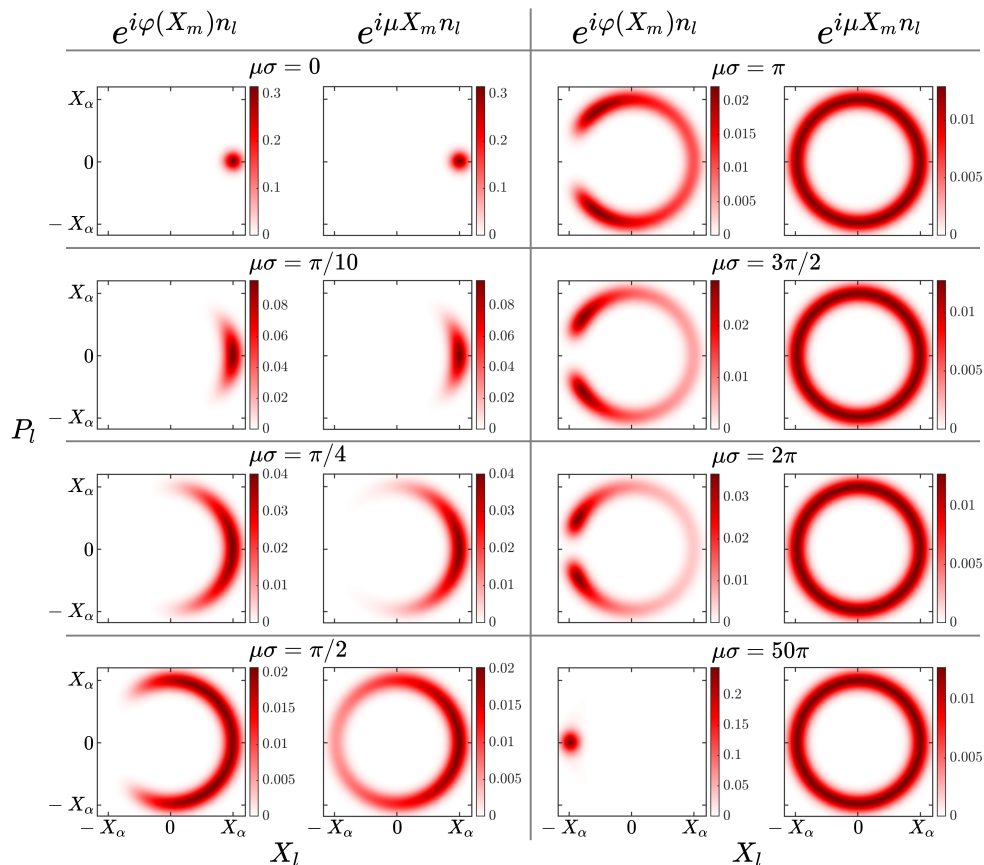


FIG. S1.  $Q$  functions of the optical state after the optomechanical interaction. Here,  $X_\alpha = 10$  and various values of  $\mu\sigma$  are shown, where  $\sigma^2$  is the initial variance of the mechanical state.  $e^{i\varphi(X_m)n_l}$  columns: the  $Q$  functions for a nonlinear optomechanical interaction that incorporates the nonlinear cavity input-output function.  $e^{i\mu X_m n_l}$  columns: the same case but with the nonlinear optomechanical unitary approximated to first order in position  $X_m$ . Note that in the expansion of  $\varphi(X_m)$ , the second order term in  $X_m$  with  $\Delta = 0$  is zero. The  $\pi$ -phase limit is seen at large optical rotations, for example at  $\mu\sigma = 50\pi$ , the optical coherent state has almost fully rotated  $\pm\pi$  in phase space. An animation of the  $Q$  function with increasing  $\mu\sigma$  is provided as a supplementary file.

#### Large $\mu\sigma$ and the $\pi$ -phase limit

For any finite value of  $X_m$ , in the limit  $\mu \rightarrow \infty$ , we have  $f_R \rightarrow -1$  and  $f_I \rightarrow 0$ . Hence, in this limit  $\mathcal{P} = F = \frac{1}{\pi} \exp[-(X_l + a_\alpha)^2 - P_l^2]$  and  $P_f(X_m) = P_i(X_m)$ . This means the optical coherent state has fully rotated  $\pm\pi$  in phase space (see Fig. S1) and no information is gained about the mechanics. More specifically, as  $\mu\sigma \rightarrow \infty$  and  $P_f(X_m) \rightarrow P_i(X_m)$ , we have  $\mathbb{E}[\sigma_f^2] \rightarrow \sigma^2$  regardless of the value of  $\zeta$ . Thus, in the high  $\mu\sigma$  limit all  $\mathbb{E}[\sigma_f^2]$  curves must approach each other, including the  $\zeta_{\text{opt}}$  and  $\zeta = 1$  curves as shown in the extended plot of  $\mathbb{E}[\sigma_f^2]$  in Fig. S2(a). However, we remind the reader that our single cavity mode treatment is only accurate for  $\mu\sigma \ll 2\mathcal{F}_c$ .

Interestingly, by extending the plot  $\mathbb{E}[\sigma_f^2]$  as in Fig. S2(a), we observe non-monotonic behaviour in the  $\mathbb{E}[\sigma_f^2]$  curve for  $\zeta = 1$  between  $\mu\sigma \approx 20$  and  $\mu\sigma \approx 30$ . This non-monotonic behaviour can be understood from the optical phase-space plots in Figs S2(b) and (c). As shown in Fig. S2(b), at  $\mu\sigma \approx 20$  a phase-quadrature measurement is effective at discriminating between the regions of anticlockwise and clockwise optical rotation, which originate from the positive and negative values of  $X_m$  from the initial mechanical distribution, respectively. Importantly, as  $\mu\sigma$  increases from  $\mu\sigma \approx 20$ , the overlap between these two regions also increases (cf. the Supplemental animation). Therefore, a phase-quadrature measurement is less effective at discriminating between different mechanical positions and thus less effective at localizing the initial mechanical state.

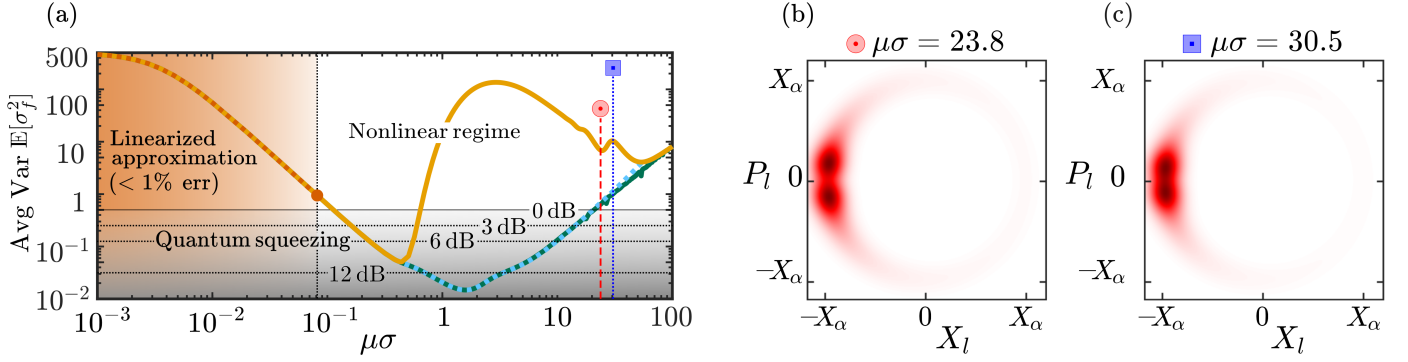


FIG. S2. (a) Extended plot of the mechanical position variance averaged over all measurement outcomes  $\mathbb{E}[\sigma_f^2]$  up to  $\mu\sigma = 100$ . Here, the  $\mathbb{E}[\sigma_f^2]$  curves for  $\zeta_{\text{opt}}$  and  $\zeta = 1$  approach each other as  $\mu\sigma$  increases. Non-monotonic behaviour is also observed for the  $\zeta = 1$  curve between  $\mu\sigma \approx 20$  and  $\mu\sigma \approx 30$ , which may be understood from the Husimi- $Q$  functions of the optical field. (b) A local minimum is located in the  $\mathbb{E}[\sigma_f^2]$  curve for  $\zeta = 1$  at  $\mu\sigma = 23.8$  (indicated by the red circle). For this value of  $\mu\sigma$ , a phase quadrature measurement can effectively discriminate between regions of anticlockwise and clockwise optical rotations, which are induced by positive and negative mechanical positions, respectively. (c) A local maximum is located in the  $\mathbb{E}[\sigma_f^2]$  curve for  $\zeta = 1$  at  $\mu\sigma = 30.5$  (indicated by the blue square). In this case, the regions of anticlockwise and clockwise optical rotations begin to significantly overlap and thus the phase-quadrature measurement performs more poorly.

### C. Gaussian approximation to pulsed measurement

#### General-dyne coordinates

By computing  $\frac{\partial F}{\partial X_m}|_{X_l, P_l} = 0$  we find

$$b_\alpha P_l f_R - a_\alpha X_l f_I + (a_\alpha^2 - b_\alpha^2) f_R f_I = 0. \quad (\text{S59})$$

We would like to expand the filtering function about its maximum to proceed with a Gaussian approximation to the general-dyne measurement. Here, we motivate the use of ‘general-dyne coordinates’. Let us first parametrize the  $f_R$  and  $f_I$  functions by a new variable  $z$ , i.e.

$$f_R(z) = \frac{1 - (z/2)^2}{1 + (z/2)^2}, \quad (\text{S60})$$

$$f_I(z) = \frac{z}{1 + (z/2)^2}. \quad (\text{S61})$$

Then, if we put  $X_l = a_\alpha f_R(z) + \delta_{X_l}$  and  $P_l = b_\alpha f_I(z) + \delta_{P_l}$  with  $\delta = \sqrt{\delta_{X_l}^2 + \delta_{P_l}^2}$  into Eq (S59) we find  $\delta_{P_l} = \frac{a_\alpha f_I}{b_\alpha f_R} \delta_{X_l}$ . Thus, we have two similar right-angled triangles with acute angle  $\psi$  satisfying

$$\sin(\psi) = \frac{a_\alpha f_I}{\sqrt{b_\alpha^2 f_R^2 + a_\alpha^2 f_I^2}} = \frac{\delta_{P_l}}{\delta}, \quad (\text{S62})$$

$$\cos(\psi) = \frac{b_\alpha f_R}{\sqrt{b_\alpha^2 f_R^2 + a_\alpha^2 f_I^2}} = \frac{\delta_{X_l}}{\delta}, \quad (\text{S63})$$

$$\tan(\psi) = \frac{a_\alpha f_I}{b_\alpha f_R} = \frac{\delta_{P_l}}{\delta_{X_l}}. \quad (\text{S64})$$

This motivates choosing the general-dyne coordinates  $(z, \delta)$  to parametrize the measurement space

$$X_l = a_\alpha f_R(z) + \delta \frac{b_\alpha f_R(z)}{\sqrt{b_\alpha^2 f_R^2 + a_\alpha^2 f_I^2}}, \quad (\text{S65})$$

$$P_l = b_\alpha f_I(z) + \delta \frac{a_\alpha f_I(z)}{\sqrt{b_\alpha^2 f_R^2 + a_\alpha^2 f_I^2}}, \quad (\text{S66})$$

with  $z \in (-\infty, +\infty)$  and  $\delta \in [-\min(a, b), \infty)$ . The Jacobian determinant for the transformation from  $(X_l, P_l)$  space to general-dyne coordinates  $(z, \delta)$  is

$$\det J = \frac{4}{4 + z^2} \left[ \sqrt{a_\alpha^2 f_I^2 + b_\alpha^2 f_R^2} + \delta \frac{a_\alpha b_\alpha}{a_\alpha^2 f_I^2 + b_\alpha^2 f_R^2} \right]. \quad (\text{S67})$$

Gaussian approximation to  $F$ ,  $P_f(X_m)$ , and  $\mathcal{P}$  for a  $(z, \delta)$  outcome

Inserting the general-dyne coordinates into Eq. (S56) and expanding to second order about the maximum of the filtering function at  $\mu X_m = z$ ,  $\delta = 0$  gives

$$F = \frac{1}{\pi} e^{-\delta^2 - \beta(\mu X_m - z)^2}, \quad (\text{S68})$$

$$\beta = \frac{16}{(4 + z^2)^2} \left[ a_\alpha^2 f_I^2(z) + b_\alpha^2 f_R^2(z) + \delta \frac{a_\alpha b_\alpha}{\sqrt{a_\alpha^2 f_I^2(z) + b_\alpha^2 f_R^2(z)}} \right]. \quad (\text{S69})$$

Within this Gaussian approximation, for an initial mechanical Gaussian state  $P_i(X_m) = e^{-X_m^2/2\sigma^2}/\sqrt{2\pi\sigma^2}$ , the output position probability distribution is given by

$$P_f(X_m) = \frac{1}{\sqrt{2\pi\sigma_f^2}} \exp \left[ -\frac{(X_m - \bar{X})^2}{2\sigma_f^2} \right], \quad (\text{S70})$$

$$\sigma_f^2 = \frac{\sigma^2}{1 + 2\mu^2\sigma^2\beta}, \quad (\text{S71})$$

$$\bar{X} = \frac{z}{\mu} \frac{2\mu^2\sigma^2\beta}{1 + 2\mu^2\sigma^2\beta}. \quad (\text{S72})$$

While the heralding probability is given by

$$\mathcal{P} = \int dX_m F(X_m) P_i(X_m) \quad (\text{S73})$$

$$= \frac{1}{\pi\sqrt{1 + 2\mu^2\sigma^2\beta}} \exp \left[ -\delta^2 - \frac{\beta}{1 + 2\mu^2\sigma^2\beta} z^2 \right]. \quad (\text{S74})$$

Averaging over all measurement outcomes  $(z, \delta)$  gives

$$\mathbb{E}[\sigma_f^2] = \int dz \int d\delta \mathcal{P}(z, \delta) |\det J| \sigma_f^2. \quad (\text{S75})$$

#### D. Optical loss

To study the effect of optical losses on the position measurement we employ a beamsplitter model for loss after the optomechanical interaction [U. Leonhardt, *Measuring the quantum state of light*, Vol. 22 (Cambridge university press, 1997)]. To this end, we introduce an extra environmental vacuum mode that interacts with the output optical mode on a beamsplitter of transmission coefficient  $\eta$ . We then consider a position-quadrature measurement  $\langle Z |$  made by the environment that will be traced over at a subsequent step. The measurement operator now becomes  $\Upsilon' = \langle Z | \langle X_I | \langle P_I | B B_\eta U | \alpha \rangle | 0 \rangle | 0 \rangle = \Theta_Z \Upsilon_\eta$  where

$$\Upsilon_\eta = \langle X_I | \langle P_I | B | \eta \alpha (f_R + i f_I) \rangle | 0 \rangle \quad (\text{S76})$$

$$\Theta_Z = \left\langle Z \left| \sqrt{1 - \eta^2} \alpha (f_R + i f_I) \right. \right\rangle, \quad (\text{S77})$$

and  $B_\eta$  is the beamsplitter modelling loss. To account for loss of information we must trace over all possible measurements the environment can make  $Z \in (-\infty, +\infty)$ . Note that as  $\Upsilon_\eta$  and  $\Theta_Z$  are both functions of the position operator  $X_m$ ,  $[\Upsilon_\eta, \Theta_Z] = 0$ , and the measurement map may be written as

$$\rho'_f = \frac{1}{\mathcal{P}'} \Upsilon_\eta \left( \int dZ \Theta_Z \rho_i \Theta_Z^\dagger \right) \Upsilon_\eta^\dagger, \quad (\text{S78})$$

with  $\mathcal{P}' = \text{tr} \left( \int dZ \Upsilon'^\dagger \Upsilon' \rho_i \right)$ .

The measurement operator in Eq. (S76) is simply the lossless operator  $\Upsilon$  of Eq. (S31) with a reduced optical amplitude  $\alpha \rightarrow \eta\alpha$ . Hence, we know the action of  $\Upsilon_\eta$  on the position distribution of our initial state and so to study the effects of optical loss on the position measurement it suffices to analyze the transformation

$$\rho'_i = \int dZ \Theta_Z \rho_i \Theta_Z^\dagger, \quad (\text{S79})$$

which can be thought of as a change in the mechanical initial state  $\rho_i$  due to optical loss by noting  $\int dZ \Theta_Z^\dagger \Theta_Z = \mathbf{1}$ . As the operator  $\Theta_Z$  is only a function of  $X_m$ ,  $P'_i(X_m) = \langle X_m | \rho'_i | X_m \rangle = \langle X_m | \rho_i | X_m \rangle = P_i(X_m)$ .



### E. Phase quadrature measurements

Despite  $\zeta_{\text{opt}}$  being close to 1 in the zoomed-in inset of Fig. 2(c), which spans  $\mu\sigma = 6.5$  to  $\mu\sigma = 10$ , the  $\mathbb{E}[\sigma_f^2]$  curves corresponding to  $\zeta_{\text{opt}}$  and  $\zeta = 1$  are still very different in Fig. 2(b). We choose to investigate the case where  $\mu\sigma \approx 7$  and  $\zeta_{\text{opt}} = 0.99$  in Fig. S3 to explain this difference. In Fig. S3(a), we study the effect of the measurement on  $P_f(X_m)$  for three different measurement outcomes (i), (ii), (iii), which are represented by the green circles in Fig. S3(b). For simplicity, we choose outcomes with  $\delta = 0$  as  $z$  is the important parameter here that quantifies the angle over which the initial coherent state ( $z = 0, \delta = 0$ ) has rotated in phase space.

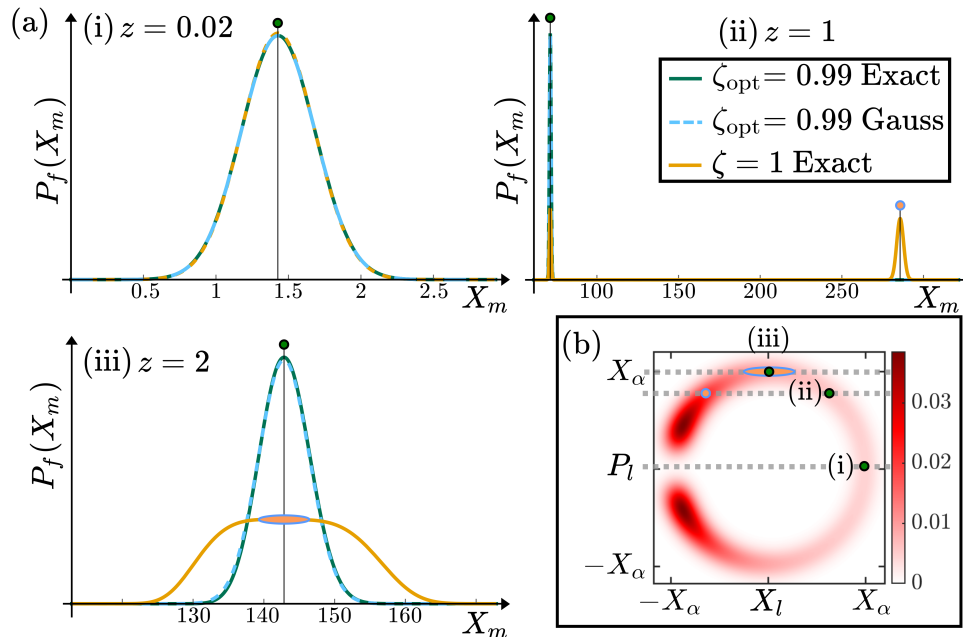


FIG. S3. Comparison of phase quadrature measurements and the optimal measurement setting. (a) The output mechanical position probability distribution  $P_f(X_m)$  for different measurement outcomes and comparing  $\zeta = 1$  with the optimal measurement setting  $\zeta_{\text{opt}}$ . Here,  $\mu\sigma \approx 7$  which gives  $\zeta_{\text{opt}} = 0.99$  and we parameterize the measurement outcomes  $(X_l, P_l)$  using the general-dyne coordinates  $(z, \delta)$ . Other parameters are the same as in Fig. 2. (i)  $(z, \delta) = (0.02, 0)$  or  $(X_l, P_l) \approx (\sqrt{1 - \zeta^2}X_\alpha, 0.02\zeta X_\alpha)$ : an outcome close to the location of the input optical coherent state  $(X_l, P_l) = (X_\alpha, 0)$  where  $\zeta_{\text{opt}}$  and  $\zeta = 1$  perform similarly. (ii)  $(z, \delta) = (1, 0)$  or  $(X_l, P_l) = (0.6\sqrt{1 - \zeta^2}X_\alpha, 0.8\zeta X_\alpha)$ : an outcome that produces a bimodal distribution when only the phase quadrature is measured. (iii)  $(z, \delta) = (2, 0)$  or  $(X_l, P_l) = (0, \zeta X_\alpha)$ : an outcome that produces a broad distribution when only the phase quadrature is measured. (b) The measurement outcomes (i), (ii), and (iii) are indicated by green circles on the phase-space of the output light. Meanwhile, the orange circle and ellipse indicate regions with the same  $P_l$  values as the measurement outcomes (ii) and (iii), respectively.

For measurement outcome (i), the performance of the optimal measurement and a phase quadrature measurement are very similar. The initial coherent state has only rotated a small angle, which may be well approximated by a phase displacement. For measurement outcome (ii), the phase quadrature measurement performs very poorly compared to the optimal measurement. The phase quadrature measurement is unable to localize the mechanical marginal to a single Gaussian peak and instead  $P_f(X_m)$  is bimodal. One peak of this bimodal distribution corresponds to the measurement outcome (ii) ( $z = 1$ ) and so is located in the same position as the narrow Gaussian produced by the optimal measurement setting  $\zeta_{\text{opt}}$ . The other peak of this distribution corresponds to the point in phase space that has the same  $P_l$  value as  $z = 1$ —as indicated by the orange circle in Fig. S3(b). The optimal measurement setting can discriminate between these two peaks by also measuring  $X_l$  quadrature. Finally, for measurement outcome (iii), the phase quadrature measurement produces a very broad  $P_f(X_m)$  distribution compared to the optimal setting. There is a broad region in the optical phase-space distribution that give the same measurement outcome of  $P_l = \zeta X_\alpha$ , which can be seen by the large region that overlaps with the orange ellipse located at  $P_l = X_\alpha$  in Fig. S3(b). Within this broad region, each phase-space point in the continuum corresponds to a different value of mechanical position  $X_m$  and as the phase quadrature measurement is poor at discriminating between these points, the mechanical state is poorly localized. The quantity  $\mathbb{E}[\sigma_f^2]$  averages over all possible measurement outcomes and by measuring both the  $X_l$  and  $P_l$  quadratures, the optimal measurement setting  $\zeta_{\text{opt}}$  avoids the contributions from the bimodal and broad distributions of Figs S3(ii) and (iii).

### F. Dependence on the detuning

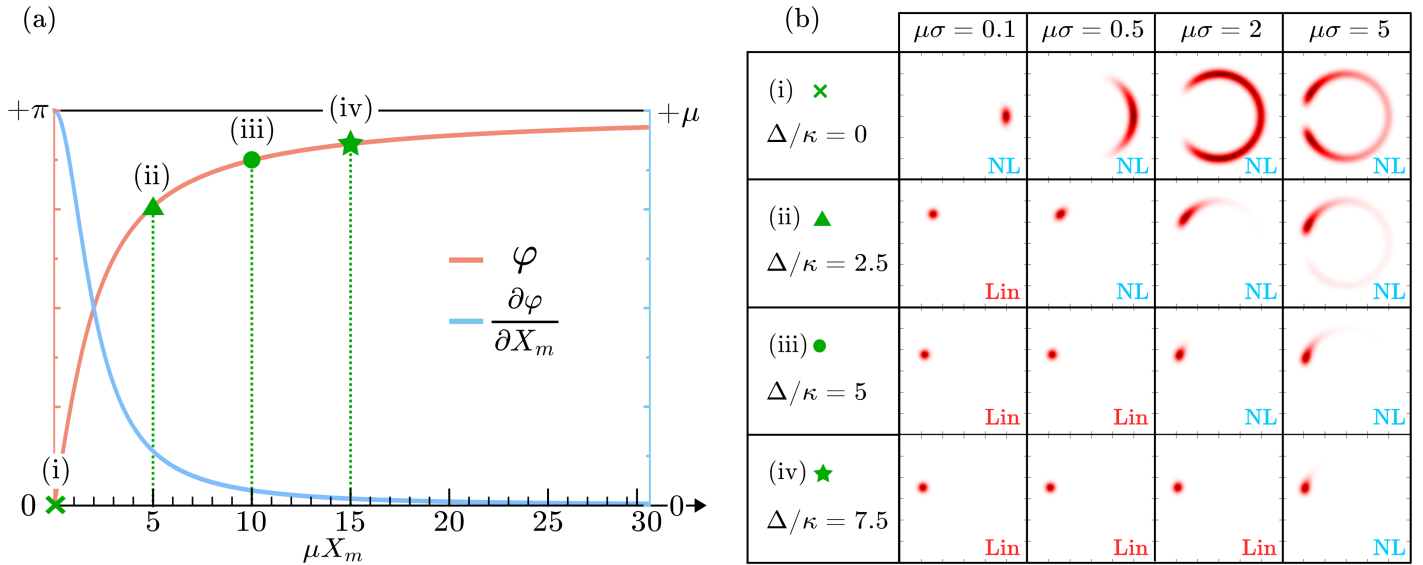


FIG. S4. Dependence of the nonlinearity condition on the detuning. (a) Plot of the optical phase  $\varphi(X_m)$  and the dimensionless mechanical momentum kick per photon  $\partial\varphi(X_m)/\partial X_m$ . Note there is a factor of 2 difference between  $\mu X_m$  and  $\Delta/\kappa$ , i.e.  $\Delta/\kappa \rightarrow \mu X_m/2$ —see the form of the nonlinear response function  $f(X_m)$ . (b) Phase-space plots of the optical pulse after the optomechanical interaction for various values of  $\mu\sigma$  and detunings  $\Delta$ . Lin: linear phase response. NL: nonlinear phase response. (i)  $\Delta/\kappa = 0$  ( $\mu X_m = 0$ ) nonlinearities are observed for  $\mu\sigma \gtrsim 0.1$ . (ii)  $\Delta/\kappa = 2.5$  ( $\mu X_m = 5$ ) nonlinearities are observed for  $\mu\sigma \gtrsim 0.5$ . (iii)  $\Delta/\kappa = 5$  ( $\mu X_m = 10$ ) nonlinearities are observed for  $\mu\sigma \gtrsim 2$ . (iv)  $\Delta/\kappa = 7.5$  ( $\mu X_m = 15$ ) nonlinearities are observed for  $\mu\sigma \gtrsim 5$ .

In Fig. 2 of the main text, we focused on the case where  $\Delta = 0$ . However, the nonlinearity condition depends on the detuning  $\Delta$  and becomes stricter as  $|\Delta|$  increases away from zero, which we explore qualitatively in Fig. S4. In Fig. S4(a), we plot the optical phase response  $\varphi(X_m)$  and the mechanical momentum kick per photon  $\partial\varphi(X_m)/\partial X_m$ . While in Fig. S4(b), we plot the optical phase space of the light after the optomechanical interaction for various values of  $\mu\sigma$  and 4 different detuning values (i)—(iv). A non-zero detuning  $\Delta$  shifts the entire  $\varphi(X_m)$  curve along the  $\mu X_m$  axis by  $-2\Delta/\kappa$ , which may be seen from the form of the nonlinear response function  $f(X_m)$ . Hence, a non-zero detuning  $\Delta$  is equivalent to shifting the origin of the phase response  $\mu X_m = 0 \rightarrow \mu X_m = 2\Delta/\kappa$  and these shifts are indicated by the green markers in Fig. S4.

In the main text we find the nonlinearity condition at (i)  $\Delta = 0$  is  $\mu\sigma \gtrsim 0.1$ . More precisely, in Fig. 2 we define the nonlinearity condition as  $\mu\sigma > 0.08$  as the linearized approximation now deviates from the exact theory by  $> 1\%$ . This nonlinearity condition is further motivated by the experiment of Ref. [G. Brawley, *et al.*, *Nat. Commun.* **7**, 10988 (2016)], which, coincidentally, achieved  $\mu\sigma = 0.08$  and observed the quadratic and higher powers of the mechanical position  $X_m$  in the optical phase shift. In Fig. S4, the case where  $\Delta = 0$  is indicated by the green cross. At this detuning value, the optical phase is most sensitive to mechanical displacements and the mechanical momentum kick per photon is maximum. Notably, the nonlinear regime can be viewed as the regime where the optical mode experiences significant optical rotations that cannot be described by the linearized approximation. In Fig. S4(b), we see the optical phase space plot already shows some significant rotations at  $\mu\sigma = 0.1$ , where mechanical information is not only encoded on solely the optical phase quadrature but also the orthogonal amplitude quadrature. Thus, we find the nonlinearity condition  $\mu\sigma \gtrsim 0.1$  just from observation of the phase space of the output optical pulse.

The next detuning value (ii)  $\Delta/\kappa = 2.5$  is indicated by the green triangle in Fig. S4. At  $\mu\sigma = 0.1$ , the corresponding phase-space plot does not show any significant optical rotations, whereas at  $\mu\sigma = 0.5$ , the optical-phase space plot begins to show significant optical rotations due to the nonlinearities. By increasing  $\Delta$  further we note that we are exploring regions of the optical phase response which are less sensitive to displacements of the mechanical position, i.e.  $\partial\varphi(X_m)/\partial X_m$  is a decreasing function of  $X_m$ . By again analyzing the phase-space plots of Fig. S4(b), we observe nonlinearities for (iii)  $\Delta/\kappa = 5$  (green circle) at  $\mu\sigma \gtrsim 2$  and for (iv)  $\Delta/\kappa = 7.5$  (green star) at  $\mu\sigma \gtrsim 5$ . Thus, the factor by which the nonlinearity condition increases is not proportional to the difference in  $\Delta/\kappa$  and this is due to the nonlinearity of the function  $\varphi(X_m)$ .

## V. CONTINUOUS MEASUREMENT

### A. Agreement with the linearized regime of optomechanics and the linearized measurement rate

For small optical rotations  $\mu\sigma \ll 1$  and zero detuning  $\Delta = 0$ ,  $c = \sqrt{2k}f(X_m) \approx \sqrt{2k} + ic_l$  with  $c_l = \sqrt{2\mu^2k}X_m$ . Using  $\mathcal{H}[c + \gamma] = \mathcal{H}[c]$  and  $\mathcal{D}[c + \gamma]\rho = \mathcal{D}[c]\rho + \frac{1}{2}[\gamma^*c - \gamma c^\dagger, \rho]$ , the nonlinear SME in Eq. (S53) returns the continuous SME from the linearized regime of optomechanics

$$d\rho = -\frac{i}{\hbar}[H_0, \rho]dt + i2\mu k[X_m, \rho]dt + \mathcal{D}[c_l]\rho dt + \sqrt{1 - \zeta^2}\mathcal{H}[ic_l]\rho dW_{X_l} + \zeta\mathcal{H}[c_l]\rho dW_{P_l}. \quad (\text{S80})$$

Here, the term  $i2\mu k[X_m, \rho]dt$  represents a *deterministic* momentum kick on the mechanical oscillator, which leads to a shift in the equilibrium mean position and is typically transformed away. Note this transformation is only valid if  $\mu\sigma \ll 1$ .

In the linearized regime, the input optical drive is large and so the Heisenberg-Langevin equation for the intracavity field Eq. (S1) can be split up into a part describing the large intracavity field  $\alpha_c$  and a part describing quantum fluctuations. In this regime, the large intracavity mean field amplitude obeys

$$\dot{\alpha}_c = +i\sqrt{2}g_0\alpha_c X_m - \kappa\alpha_c + \sqrt{2\kappa}\alpha_{in}, \quad (\text{S81})$$

where the input photon flux is  $|\alpha_{in}|^2 = 2k$  as  $|\alpha|^2 = |\alpha_{in}|^2 dt$ . Then for small optical rotations  $\mu^2\sigma^2 \sim 2g_0^2 \langle X_m^2 \rangle / \kappa^2 \ll 1$  the equation for this large amplitude is well approximated by

$$\dot{\alpha}_c = -\kappa\alpha_c + \sqrt{2\kappa}\alpha_{in} \quad (\text{S82})$$

with steady state solution  $\kappa|\alpha_c|^2 = 2|\alpha_{in}|^2$ . Therefore, we have that  $k = \frac{\kappa|\alpha_c|^2}{4}$ . Using  $\mu = \sqrt{8}g_0/\kappa$  and  $g = |\alpha_c|g_0$ , we arrive at an expression for the measurement rate which is *only* true in the linearized regime of optomechanics

$$\mu^2 k = k_l = \frac{2g^2}{\kappa}. \quad (\text{S83})$$

However, beyond the linearized regime Eq. (S83) is *not* valid. Note that many authors include an additional factor of 2 in their definition of  $k_l$  by defining  $\kappa$  as an intensity quantity and if one includes optical loss into the definition, this rate becomes  $k_l = 2\eta g^2/\kappa$ . Furthermore, in the linearized regime we can rewrite  $2\mu k = \sqrt{2}g_0|\alpha_c|$  in Eq. (S80) to write the deterministic momentum kick term in a more familiar form.

### B. Stochastic Gaussian measurement regime

We write  $\mu X_m = \mu \langle X_m \rangle + \mu Y_m$ , which is valid at every time step  $t \rightarrow t + dt$  in the SME. Then we may expand  $c$  to first order in  $\mu Y_m$  if  $\langle \mu Y_m \rangle^2 \sim \text{Var}(\mu Y_m) \ll 1$ . Importantly, the infinitesimal phase shifts  $\mu Y_m$  over each  $t \rightarrow t + dt$  may integrate to arbitrarily large optical rotations  $\mu\sigma$  over a finite duration. To first order in  $\mu Y_m$ ,

$$c = \sqrt{2k}f(\langle X_m \rangle) + \frac{ic_l}{[1 - i(\frac{\mu}{2}\langle X_m \rangle + \frac{\Delta}{\kappa})]^2} \quad (\text{S84})$$

with  $c_l = c_l^\dagger = \sqrt{2\mu^2k}Y_m$ . The measurement records are therefore

$$dy_{X_l} = f_R(\langle X_m \rangle)dt + \frac{dW_{X_l}}{\sqrt{8\eta_{X_l}(1 - \zeta^2)k}}, \quad (\text{S85})$$

$$dy_{P_l} = f_I(\langle X_m \rangle)dt + \frac{dW_{P_l}}{\sqrt{8\eta_{P_l}\zeta k}}, \quad (\text{S86})$$

as by definition  $\langle Y_m \rangle = 0$ . The difference with expressions for  $dy_{X_l}$  and  $dy_{P_l}$  in the main text is in taking the expectation value of  $X_m$  before entering it into the functions  $A$  and  $B$ . The measurement currents are defined in the same way as in the general nonlinear theory.

Expanding the SME of Eq. (S53) to first order in  $\mu Y_m$  gives

$$d\rho = -\frac{i}{\hbar}[H_0 + H_1, \rho]dt + \mathcal{D}\left[\frac{c_l}{1 + (\frac{\mu}{2}\langle X_m \rangle + \frac{\Delta}{\kappa})^2}\right]\rho dt + \sqrt{1 - \zeta^2}\mathcal{H}\left[\frac{ic_l}{[1 - i(\frac{\mu}{2}\langle X_m \rangle + \frac{\Delta}{\kappa})]^2}\right]\rho dW_{X_l} + \zeta\mathcal{H}\left[\frac{c_l}{[1 - i(\frac{\mu}{2}\langle X_m \rangle + \frac{\Delta}{\kappa})]^2}\right]\rho dW_{P_l}, \quad (\text{S87})$$

where the term  $H_1$  now describes a *stochastic* momentum kick, explicitly given by

$$\frac{H_1}{\hbar} = -\frac{2\mu k}{1 + \left(\frac{\mu}{2}\langle X_m \rangle + \frac{\Delta}{\kappa}\right)^2} Y_m. \quad (\text{S88})$$

This momentum kick is stochastic due to the denominator in Eq. (S88), which originates from the nonlinear cavity input-output function. Therefore to study the effect of this term, we do not transform it away by shifting the  $X_m$  and  $P_m$  coordinates. Furthermore as  $\mu \langle X_m \rangle / 2 + \Delta / \kappa \rightarrow \infty$ , Eq. (S87) tends towards  $d\rho = -i[H_0/\hbar, \rho]dt$  as the light is no longer resonant with the cavity and is simply reflected at the input.

Adding mechanical decoherence and optical loss to Eq. (S87) and using  $\mathcal{D}[c + \gamma]\rho = \mathcal{D}[c]\rho + \frac{1}{2}[\gamma^*c - \gamma c^\dagger, \rho]$  gives

$$\begin{aligned} d\rho = & -\frac{i}{\hbar}[H_0 + H_1 + H_2, \rho]dt + \mathcal{D}\left[\frac{c_l}{1 + \left(\frac{\mu}{2}\langle X_m \rangle + \frac{\Delta}{\kappa}\right)^2}\right]\rho dt + \mathcal{D}[L_Y]\rho dt \\ & + \sqrt{(1 - \zeta^2)}\eta_{X_l}\mathcal{H}\left[\frac{ic_l}{\left[1 - i\left(\frac{\mu}{2}\langle X_m \rangle + \frac{\Delta}{\kappa}\right)\right]^2}\right]\rho dW_{X_l} + \zeta\sqrt{\eta_{P_l}}\mathcal{H}\left[\frac{c_l}{\left[1 - i\left(\frac{\mu}{2}\langle X_m \rangle + \frac{\Delta}{\kappa}\right)\right]^2}\right]\rho dW_{P_l}, \end{aligned} \quad (\text{S89})$$

where  $H_2/\hbar = -\gamma \langle X_m \rangle P_m$  and  $L_Y = \sqrt{\frac{4\gamma k_b T}{\hbar\omega_m}}Y_m + i\sqrt{\frac{\hbar\omega_m\gamma}{4k_b T}}P_m$ , which as before models quantum Brownian motion .

### Stochastic Riccati equations

Here, we follow [J. Zhang and K. Mølmer, *Phys. Rev. A* **96**, 062131 (2017)] to cast Eq. (S89) into a system of stochastic differential equations (SDEs), but we also include a linear term in the Hamiltonian, accounted for by the displacement vector  $\mathbf{d}$ . Defining the vector  $\mathbf{r} = (Y_m, P_m)^\top$  we can rewrite the Hamiltonian  $H = H_0 + H_1 + H_2$  in Eq. (S89) as

$$H/\hbar = \frac{1}{2}\mathbf{r}^T R \mathbf{r} + \mathbf{d}^T \Omega \mathbf{r}, \quad (\text{S90})$$

$$R = \omega_m \mathbf{1}, \quad (\text{S91})$$

$$\mathbf{d} = \begin{pmatrix} -\gamma \langle X_m \rangle & 2\mu k \\ -\omega_m \langle X_m \rangle + \frac{2\mu k}{1 + \left(\frac{\mu}{2}\langle X_m \rangle + \frac{\Delta}{\kappa}\right)^2} \end{pmatrix}, \quad (\text{S92})$$

$$\Omega = \begin{pmatrix} 0 & 1 \\ -1 & 0 \end{pmatrix}. \quad (\text{S93})$$

Then writing the three independent measurement output operators in Eq. (S89) as a vector  $\mathbf{c} = C\mathbf{r}$  with

$$C = \begin{pmatrix} C_{11} & 0 \\ C_{21} & 0 \\ C_{31} & C_{32} \end{pmatrix}, \quad (\text{S94})$$

$$C_{11} = \frac{i\sqrt{2\mu^2 k(1 - \zeta^2)}}{\left[1 - i\left(\frac{\mu}{2}\langle X_m \rangle + \frac{\Delta}{\kappa}\right)\right]^2}, \quad (\text{S95})$$

$$C_{21} = \frac{\sqrt{2\mu^2 k\zeta^2}}{\left[1 - i\left(\frac{\mu}{2}\langle X_m \rangle + \frac{\Delta}{\kappa}\right)\right]^2}, \quad (\text{S96})$$

$$C_{31} = \sqrt{\frac{4\gamma k_b T}{\hbar\omega_m}}, \quad (\text{S97})$$

$$C_{32} = i\sqrt{\frac{\hbar\omega_m\gamma}{4k_b T}}. \quad (\text{S98})$$

Furthermore, we define the efficiency matrix  $\boldsymbol{\eta} = \text{diag}(\eta_{X_l}, \eta_{P_l}, 0)$  and the vector of Wiener increments  $d\mathbf{W} = (dW_{X_l}, dW_{P_l}, 0)^\top$ . We then introduce the drift matrix  $M$ , the diffusion matrix  $D$ , and the noise matrix  $N$

$$M = \Omega (R + \text{Im}[C^\dagger(t)C(t)]), \quad (\text{S99})$$

$$D = -\Omega \text{Re}[C^\dagger(t)C(t)]\Omega, \quad (\text{S100})$$

$$N = 2V\text{Re}[C^\top(t)] - \Omega \text{Im}[C^\top(t)], \quad (\text{S101})$$

$$(\text{S102})$$

and we find that—given an initial Gaussian mechanical state—the dynamics described by Eq. (S89) can be completely described by 5 independent SDEs. Namely, two SDEs describing the evolution of the first moments

$$d\langle \mathbf{r} \rangle = (M \langle \mathbf{r} \rangle + \mathbf{d}) dt + N \sqrt{\eta} d\mathbf{W} \quad (\text{S103})$$

and a stochastic Riccati matrix equation describing the evolution of the 3 independent covariance matrix elements  $V$

$$\frac{dV}{dt} = MV + VM^T + D - N\eta N^T, \quad (\text{S104})$$

where  $V_{i,j} = \frac{1}{2} \langle \{r_i, r_j\} \rangle - \langle r_i \rangle \langle r_j \rangle$ . As opposed to linearized optomechanics, the Riccati equation is no longer deterministic. The origin of this stochasticity comes from the dependence of the measurement output operators  $\mathbf{c}$  on the stochastic mean position  $\langle X_m \rangle$ . Furthermore, note that the covariance matrix is invariant under the transformation  $X_m = \langle X_m \rangle + Y_m$  at each time step, i.e.  $V_X = \langle X_m^2 \rangle - \langle X_m \rangle^2 = \langle Y_m^2 \rangle - \langle Y_m \rangle^2$  and  $V_{XP} = \langle \{X_m, P_m\} \rangle / 2 - \langle X_m \rangle \langle P_m \rangle = \langle \{Y_m, P_m\} \rangle / 2 - \langle Y_m \rangle \langle P_m \rangle$ .

### C. Drive-locking

#### *No feedback case*

Choosing the same parameters as in the main text, we run the simulations for the stochastic Gaussian regime again but without feedback to the drive field, which produces the results shown in Fig. S5. Comparison with Fig. 3 confirms our choice of feedback in the main text removes the asymmetry in the optical phase space distribution and improves the mechanical squeezing. Furthermore, in Fig. S5 we see the evolution of the means becomes harmonic again. This is because without feedback, the intracavity power is lower and so (for these specific parameters) the higher order terms in  $X_m$  in the optical force are not present. However, in principle arbitrarily high orders in  $X_m$  are present in the optical force in the nonlinear theory for *both* with and without drive-locking. Inserting Eq. (S6) into Eq. (S3), we see that the dimensionless optical force is given by the right hand side of

$$\dot{P}_m = \frac{\mu a_{in}^\dagger a_{in}}{1 + \left(\frac{\mu}{2} X_m + \frac{\Delta}{\kappa}\right)^2}. \quad (\text{S105})$$

By expanding this optical force in  $X_m$ , we see that the contributions for a given order of  $X_m$  depend on  $\Delta/\kappa$ ,  $\mu$ , and the intracavity power via the input field operators  $a_{in}$ .

To gain further insight we may also take the real Fourier transform of the mean mechanical position  $\mathcal{F}\{\langle X_m \rangle\}$ . For no feedback, this is shown in Fig. S6(a) for a given trajectory. Here, we see a peak in  $\mathcal{F}\{\langle X_m \rangle\}$  at a higher frequency than  $\omega_m$ , which is a demonstration of the optical spring effect due to an  $X_m$ -dependent term in the optical force, i.e. an  $X_m^2$ -dependent term in an effective Hamiltonian.

#### *Feedback to the drive field*

Fig. S6(b) shows  $\mathcal{F}\{\langle X_m \rangle\}$  for a particular trajectory but now when the detuning of the drive is chosen to cancel the slowly-varying component of  $\langle X_m \rangle$ , which symmetrizes the optical phase space distribution as in the main text. Let this low frequency component of the mean mechanical position be  $\overline{\langle X_m \rangle}$ . Then, it follows that the portion of  $\mathcal{F}\{\langle X_m \rangle\}$  which is captured by the third-order Butterworth filter corresponds to  $\mathcal{F}\{\overline{\langle X_m \rangle}\}$ . Therefore, by calculating  $\mathcal{F}\{\langle X_m \rangle\}$  at each time step, the low-pass filtering allows one to calculate  $\overline{\langle X_m \rangle}$  at each time step too. From Eq. (S89), for example, we can identify the correct choice of feedback to cancel the low frequency components is

$$\Delta = -\frac{1}{2} \mu \kappa \overline{\langle X_m \rangle}. \quad (\text{S106})$$

In this way, the drive is locked to the cavity frequency, which changes as the time averaged mean mechanical position drifts away from zero. As a reminder,  $\Delta$  is defined as the detuning from the cavity resonance for  $X_m = 0$ . However, in our numerical simulations, or indeed an experiment, this cancellation of  $\overline{\langle X_m \rangle}$  must be done in a causal fashion, such that only information about  $\mathcal{F}\{\langle X_m \rangle\}$  at times  $t' < t$  is used to compute the detuning  $\Delta$  at time  $t$ .

Fig. S6(b) contains a peak in  $\mathcal{F}\{\langle X_m \rangle\}$  at  $\omega_m$ , which shows that the optical spring effect is cancelled by the drive-locking. Furthermore, this figure shows a small peak in  $2\omega_m$  as higher frequency components are now amplified, which comes from an  $X_m^2$  term in the optical force. This  $2\omega_m$  component explains the anharmonicity in the evolution of the means in Fig. 3. We note that the order and cutoff frequency of the Butterworth are chosen to optimize the run time of the numerical simulations, while still demonstrating the working principle of the stochastic Gaussian regime. Choosing the optimal filtering procedure and choice of  $\Delta$  depends on an experimental implementation.

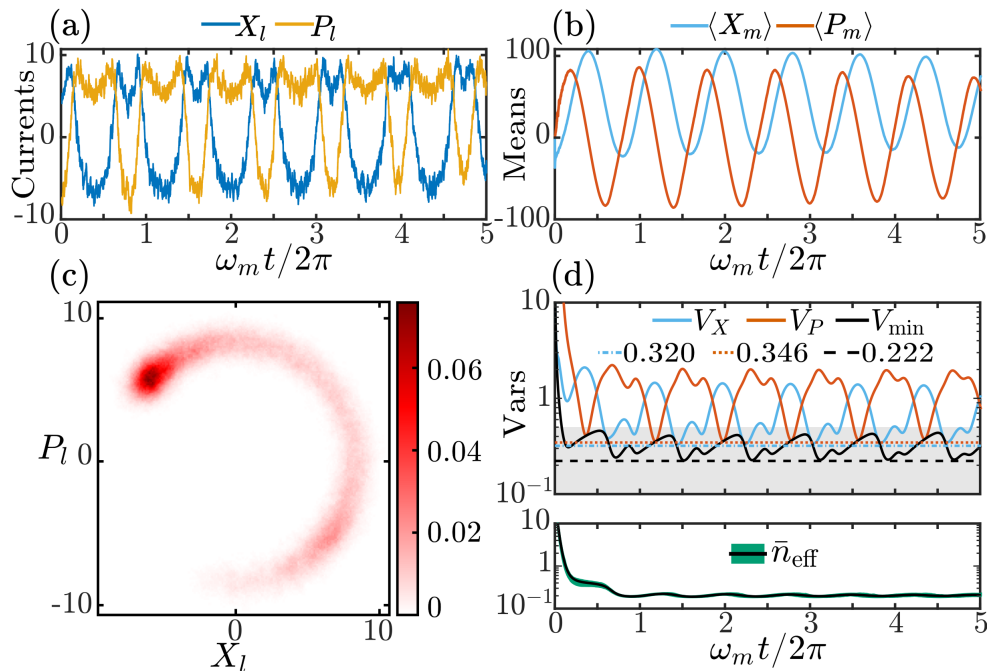


FIG. S5. Continuous position measurement in the stochastic Gaussian regime without feedback. Here,  $X_\alpha/\sqrt{2} = 10$ ,  $\omega_m/2\pi = 10$  MHz,  $\mu = 0.05$ ,  $\mu^2 k/\omega_m = 2$ ,  $\eta = 0.7$ ,  $\gamma/2\pi = 10$  Hz,  $\zeta = 1/\sqrt{2}$ ,  $T = 4$  K and the initial mechanical state is at 100 mK. The general-dyne measurement currents  $X_l$  and  $P_l$  plotted as a function of time for a given stochastic trajectory. (b) The corresponding trajectories of the mechanical means  $\langle X_m \rangle$  and  $\langle P_m \rangle$ . (c) The same general-dyne currents plotted as a 2D histogram, normalized to one. We see that the optical phase shift averaged over this trajectory is positive. (d) Top: The position variance  $V_X$ , the momentum variance  $V_P$ , and the generalized squeezing variance  $V_{\min}$  for the same trajectory. Here, the dashed lines correspond to the mean of the minimum of each variance quantity over 100 runs, while the grey shaded area corresponds to quantum squeezing. Bottom: The effective thermal occupation  $\bar{n}_{\text{eff}}$  plotted as a function of time averaged over 100 stochastic trajectories. The shaded green area indicates the upper and lower quartile range of the 100 trajectories.

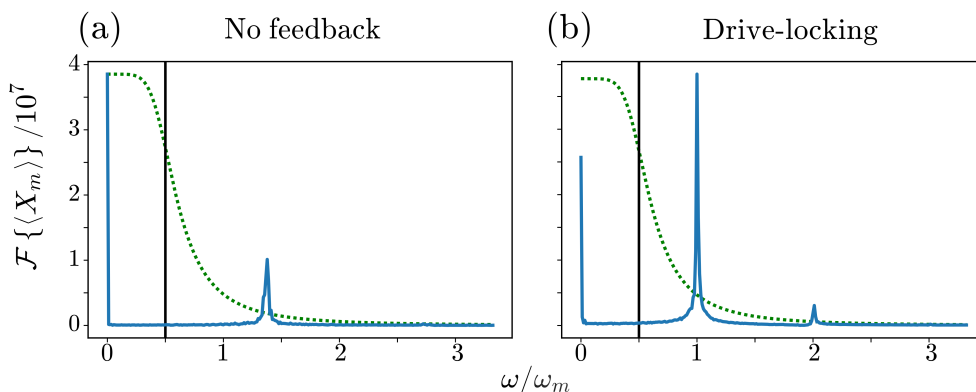


FIG. S6. Real Fourier transform of the mean mechanical position  $\mathcal{F}\{\langle X_m \rangle\}$  with (a) no drive feedback and with (b) drive-locking:  $\Delta = -\frac{1}{2}\mu\kappa\langle X_m \rangle$ . Here,  $X_\alpha/\sqrt{2} = 10$ ,  $\omega_m/2\pi = 10$  MHz,  $\mu = 0.05$ ,  $\mu^2 k/\omega_m = 2$ ,  $\eta = 0.7$ ,  $\gamma/2\pi = 10$  Hz,  $\zeta = 1/\sqrt{2}$ ,  $T = 4$  K and the initial mechanical state is a thermal state at 100 mK. A third-order Butterworth filter is shown by the green-dashed line. Meanwhile, the frequency cutoff at  $0.5\omega_m$  of the Butterworth is shown by the vertical black line and the mechanical frequency  $\omega_m$  is shown by the vertical dashed line. In (b), the Butterworth is used to calculate the detuning at each timestep. The numerical simulations last 100 mechanical periods and the real Fourier transforms are calculated with data obtained in the last 90 periods to avoid the transient effects associated with the response time of the filter.

#### D. Experimental parameters for sliced-photonic crystal devices

Here we run simulations for the stochastic Gaussian regime using different parameter sets, which are given in table I. Device A corresponds to the parameters chosen in the main text—see Figs 3, S5, and S6. Devices B and C represent smaller improvements to current state-of-art parameters for sliced-photonic crystal devices, which are given in the last column of table I. Fig. S7 shows the results of these simulations for devices B and C. In both cases, quantum squeezing is

still possible, i.e.  $V_{\min} < 1/2$ , and it is interesting to note that drive-locking is needed for the mean of the minimum value of  $V_X$  to go below  $1/2$ .

TABLE I. **Sliced-photonic crystal parameters for devices A, B, and C and the current state-of-the-art.** Device A corresponds to improvements of the current state-of-the-art—see Figs 3, S5, and S6. Devices B and C—see Fig. S7—represent smaller improvements. In the final column we give a parameter set for a current sliced-photonic crystal experiment [P. Neveu *et al.*, *In preparation* (2022)], which builds on Refs [R. Leijssen *et al.*, *Nat. Commun.* **8**, 16024 (2017); J. T. Muhonen *et al.*, *Phys. Rev. Lett.* **123**, 113601 (2019)].

Parameter	Device A	Device B	Device C	Current experiment
Mechanical frequency $\omega_m/2\pi$	10 MHz	10 MHz	10 MHz	3.6 MHz
Cavity amplitude decay rate $\kappa/2\pi$	5 GHz	5 GHz	10 GHz	10 GHz
Optomechanical coupling rate $g_0/2\pi$	90 MHz	90 MHz	35 MHz	25 MHz
Intrinsic mechanical decay rate $\gamma/2\pi$	10 Hz	100 Hz	20 Hz	20 Hz
Nonlinear optomechanical coupling strength $\mu$	0.050	0.050	0.010	0.007
Measurement efficiency $\eta$	0.70	0.50	0.25	0.25

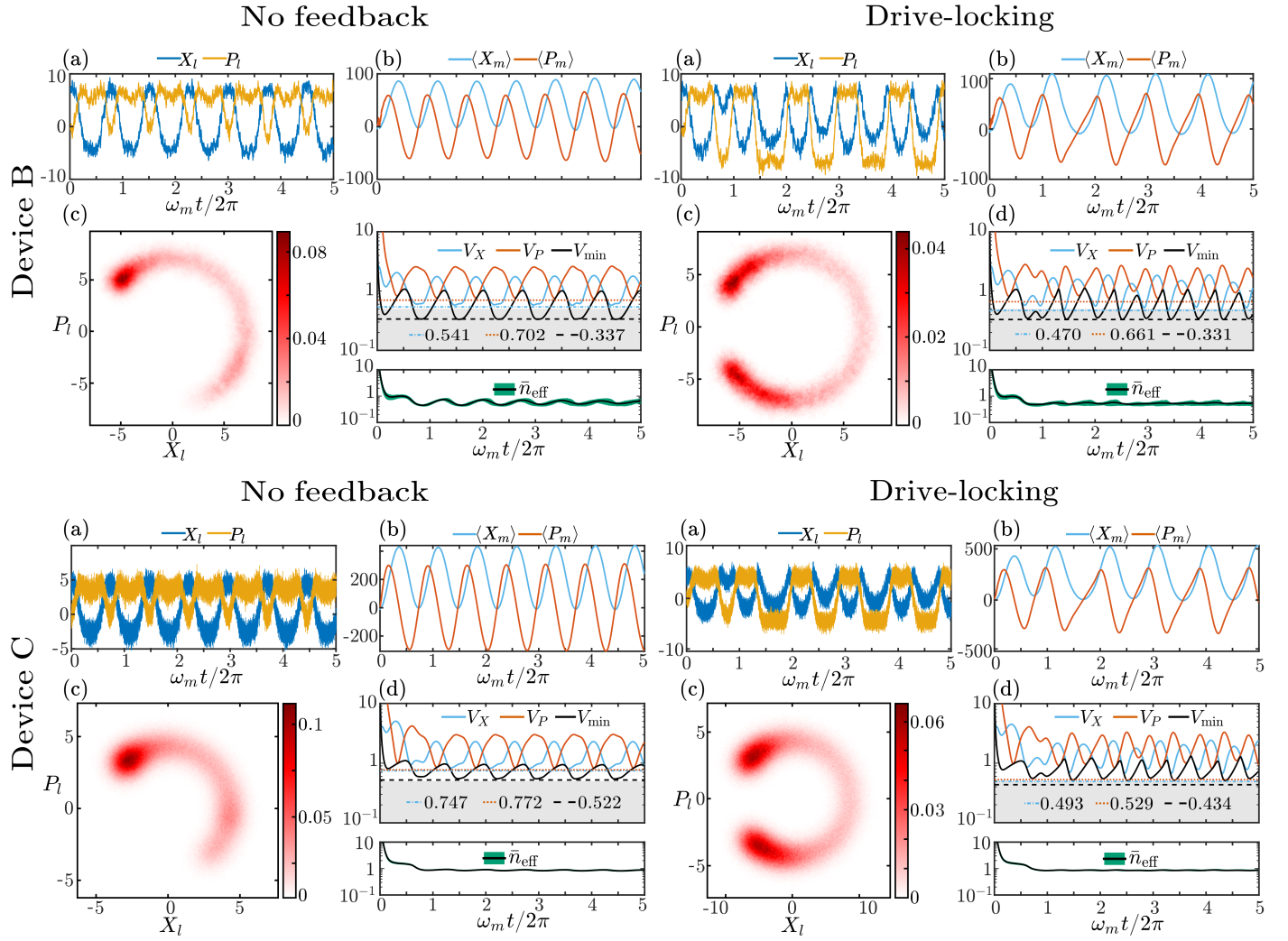


FIG. S7. Devices B and C in the stochastic Gaussian regime. Left hand side: no drive feedback. Right hand side: drive-locking  $\Delta = -\frac{1}{2}\mu\kappa\langle X_m \rangle$ . Device B:  $\eta = 0.5$ ,  $\gamma = 100\text{Hz}$ , and  $\mu = 0.05$ . Device C:  $\eta = 0.25$ ,  $\gamma = 20\text{Hz}$ , and  $\mu = 0.01$ . In both cases  $\omega_m/2\pi = 10\text{MHz}$ ,  $\mu^2 k/\omega_m = 2$ ,  $\zeta = 1/\sqrt{2}$ ,  $T = 4\text{K}$ , and the initial mechanical state is a thermal state at  $100\text{mK}$ . Here, the dashed lines correspond to the mean of the minimum of each variance quantity over 100 runs, each lasting 100 mechanical periods, while the grey shaded area corresponds to quantum squeezing.